Archaeological and Anthropological Sciences (2021) 13:203
https://doi.org/10.1007/s12520-021-01444-8

ORIGINAL PAPER

Investigation of provenances of Early Islamic lead glazes from northern Central Asia using elemental and lead isotope analyses

Catherine Klesner[1,2] · Virginie Renson[3] · Yeraly Akymbek[4,5] · David Killick[6]

Received: 13 May 2021 / Accepted: 7 September 2021

Abstract
A representative collection of Early Islamic glazed ceramics from eleven sites in southern Kazakhstan were characterized by compositional ($n=95$) and lead isotope analysis ($n=33$). The ceramics, which date from the 9–15th c. CE were examined to determine the glaze type, colorants, and opacifiers used by local craftsmen. Several distinct glaze types are present including transparent high-lead glaze ($n=66$) and opaque high-lead glaze ($n=10$), of which tin-opacified glazes, tin- and antimony-opacified glazes, and antimony-opacified glazes were all identified. The occurrence of antimony-opacified glazes and tin- and antimony-opacified glazes is unattested in this region in the Early Islamic Period and indicates that the local craftsmen in southern Kazakhstan are innovating in their production of opaque glazed ceramics using local raw materials. Lead isotope analysis was employed to identify potential sources of lead, and the results indicate that the craftsmen were obtaining lead from at least two different sources for their glazed production. Using a large comparative database and through the application of Euclidean distance, we were able to identify potential ore deposits from the Central Asian Orogenic Belt, including deposits that were active silver mines during the Medieval Period. These ore sources were local and suggest that potters were obtaining lead for glaze production from within larger acquisition networks. One cluster of samples ($n=8$) had a distinct isotopic signature that matched a unique deposit in Xinjiang, China, which indicates craftsmen were not strictly using local sources, but also obtaining lead through long-distance trade networks.

Keywords Lead isotope analysis · Early Islamic ceramics · Lead glaze · LA-ICP-MS · EPMA · Silk Road

Introduction

The Semirechye region and adjacent river valleys (Syr Darya, Talas, and Chu) along the northern edge of the Tian-shan mountains have served as an avenue for long-distance trade for millennia. This region, which is located in modern-day southern Kazakhstan and northern Kyrgyzstan, forms a narrow corridor between the major glaciated mountain ranges of Central Asia and the vast steppe. In the 6th c. CE, trade intensified over this northern branch of the Silk Road and the following six centuries were a period of political, economic, and cultural change. Archaeological sites from this time provide valuable insights into this trade as well as the economies and technologies of the supporting communities (Henshaw 2010). By examining the material remains from these sites, it is possible to reconstruct both ancient trade networks and the technological and knowledge networks that were facilitated by the increased interactions occurring along these paths.

Glazed ceramics, due to their abundance and durability, provide an excellent window through which to examine these networks. During the Early Islamic Period, increased innovation occurred in glazed ceramic technology as it became significant for economic competition in the long-distance trade networks (Mason 1995). Lead-glazed ceramics are one

✉ Catherine Klesner
klesnerc@nyu.edu

1 Department of Materials Science and Engineering, University of Arizona, Tucson, AZ, USA

2 Institute for the Study of the Ancient World, New York University, New York, NY, USA

3 Archaeometry Laboratory, Research Reactor Center, University of Missouri, Columbia, MO, USA

4 Laboratory of Archaeological Technologies, Institute of Archaeology Named A.Kh. Margulan, Almaty, Kazakhstan

5 Al-Farabi Kazakh National University, Almaty, Kazakhstan

6 School of Anthropology, University of Arizona, Tucson, AZ, USA

Published online: 24 October 2021

of the most defining features of the archaeological record in the Islamic world (Watson 2004). In the 8–12th c. CE, the widespread production and trade of lead-glazed ceramics extends from Southwest Asia into Central Asia and was centered in prosperous Silk Road cities (Henshaw 2010). In the southern Kazakhstan, there was no local glazing tradition before the Early Islamic Period (Heinsch et al. 2018), and the first local glazed ceramic production began in the 9th c. CE. Analysis of the ceramic technology from Central Asia has suggested that the technology was derivative of western Islamic traditions and potentially even directly introduced by immigrant craftsmen patronized by the emerging governing elites in eastern cities such as Nishapur, Merv, and Samarkand (Henshaw 2010). An increase in research focused on the lead-glazed ceramics produced in the eastern Islamic world (Central Asia and Iran) from the 8–12th c. CE has helped define this technology (Henshaw et al. 2006; Henshaw 2010; Bouquillon et al. 2012; Shen 2017; Holakooei et al. 2019; Martínez Ferreras et al. 2019; Molera et al. 2020), but a few studies have focused on the provenance of the glazed ceramics and the identification of the raw materials used to produce the high-lead glazes.

Lead isotope analysis in glaze studies

Lead isotope analysis (LIA) has been used as an analytical technique to help identify ore sources for the lead found in a variety of archaeological materials for the past 50 years (Pollard et al. 2007, p. 192). In recent decades, the technique has been successfully applied to lead-glazed ceramics to identify potential sources of lead ore and to give insights into the production technology (Mason et al. 1992; Wolf et al. 2003; Stos-Gale 2004; Walton 2004; Marzo et al. 2009; Cui et al. 2010; Walton and Tite 2010; Huntley et al. 2012; Thibodeau et al. 2013; Shen et al. 2019; Medeghini et al. 2020). These studies have been widely applied to include analysis of lead-glazed ceramics from the American southwest, Roman and Medieval Period ceramics from the Mediterranean, and Tang period ceramics from China.

Some of the earliest applications of lead isotope analysis on glazed ceramics were on Early Islamic Period ceramics, which are well suited for the technique as they are known to both be a widely traded commodity and there being historical documentation of the long-distance trade of lead to produce glaze and glass. This coupled problem was first investigated by Mason et al. (1992), who examined eight lead-glazed ceramics from Yemen, Iraq, Egypt, and Iran dating from the 8 to the 16th c. CE. While the small sample size only allowed for preliminary conclusions to be drawn, the results suggested that the sources for lead in the glaze were very distant from the location of ceramic production, indicating the potential for long-distance trade of lead or lead-frit for glaze production. Wolf et al. (2003) similarly examined a group of Islamic lead-glazed pottery from Fustat, Egypt, that date to the 8 to 14th c. CE. They determined that the lead used in the glaze production was obtained from distant ore sources and that a temporal change occurred in the preferred lead sources for lead-glazed ceramics. Interestingly, at no point in their period of study were local ore sources used (Wolf et al. 2003). Shen (2017), in her study of Chinese Tang dynasty *sancai* ceramics, analyzed one lead-glazed sample from Al-Raqqa in Syria (dated 8–9th c. CE) and six glazes samples from Iraq (8–14th c. CE) by LIA, and compared the data to the lead isotope data of ore deposits from the regions of Central Iran, Anatolia, Tunisia, Southwest Spain, and Sardinia. While no ore deposit was found to be a potential source for the sample from Syria, ore deposits from Iran, Tunisia, Anatolia, Spain, and Sardinia were identified as possible ore sources for the samples from Iraq. While Shen notes that her case study may reflect the trade of lead between the Middle East and the Mediterranean, including Iraqi glaze production sourcing lead from Sardinia and Spain, the overlapping of isotopic signature and small number of samples makes it impossible to associate the lead used in glaze making with a specific lead ore source. LIA has also been applied to the 11th c. CE Islamic lead-glazed ceramics from the Iberia, which indicated that craftsman were using different lead sources for the production of transparent and opaque lead glazes (Marzo et al. 2009).

These initial studies present the possibility that in the Islamic world, craftsmen were sourcing the lead for glazed ceramic production from long-distance trading networks, and not necessarily exploiting local sources. This picture is reinforced by contemporary Islamic writers. The famed geographer al-Idrisi (1154 CE) wrote that the lead from Yazd (located in Central Iran) was "traded far and wide." Abu'l Qasim Kashani (1301 CE), who was from one of the leading ceramic families in Kashan, describes the production of glazed ceramics in Iran in his *Treatise on Ceramics* (Allan 1973; Watson 2004). He describes in detail where the best raw materials for glazed ceramics were sourced, from clays and quartz to colorants, lead, and tin. Lead was noted to be imported from many places, including Kirman and Yazd in modern-day Iran, Rum, which is understood to be Anatolia and is described as the worst type of lead, and Bulghars, which is assumed to be north of the Caucasus' and is mentioned as the best type of lead (Allan 1973). Tin was also mentioned to be imported from distant locations, including Farangistan (Europe) where the tin was cast in the form of snakes, China, where it was brought in large pieces, and from the border region with the Bulghars, which again was identified as the best source (Allan 1973).

Research objectives

The paper is part of a larger study of glazed ceramics from southern Kazakhstan, which aims to characterize the provenance and technology of finely decorated glazed pottery from northern Central Asia. Our larger goals include determining the scale of local production and long-distance trade of ceramics from the 9 to 15th c. CE and the extent of local technological innovations and to identify the source of raw materials used by local craftspeople to produce the glazed wares. Through the examination of ceramic provenance and technological analysis of local and non-local ceramics, we aim to better understand both the physical trade networks in place in northern Central Asia during the 9–15th c. but also how technologies were transmitted and adapted.

A preliminary study of the chemical compositions of the ceramic pastes and glazes on thirty-nine glazed ceramics from seven sites in southern Kazakhstan indicated that, while there were distinct compositional groups for the ceramic pastes, no difference in the major, minor, or trace element concentrations in the glaze chemistries were revealed (Klesner et al. 2019; Klesner 2021). The compositional groups for the ceramic pastes suggested that around half of the glazed ceramics were non-local products brought into the region through Silk Road trade, while approximately thirty percent of the glazed wares were identified as locally produced at the site of Aktobe. Full information on the provenance of samples included in this study can be found in Klesner (2021, pp. 128–139). The local wares were stylistically indistinguishable from the imported wares, and further analysis of the glazing technology at one site, Aktobe (Klesner et al. 2021), indicates the direct adoption of the lead-glazing technology from the eastern Islamic world into southern Kazakhstan in the 9th c. CE. Given the chemical homogeneity of the lead glazes and the attested long-distance trade of lead ore and/or lead frit to produce lead glaze in the Islamic world, the following question is raised: were potters in northern Central Asia using local raw materials, particularly local lead ores sources, to produce the high-lead glaze, or was there an active long-distance trade of lead ore or lead-frit in the Islamic period?

To further understand the ceramic production and exchange in northern Central Asia, the objectives of this paper are to (1) characterize the glazes, colorants, and opacifiers used by local craftsmen on a wider array of ceramic wares from major and minor sites across southern Kazakhstan and (2) identify the sources of lead used in the production of the high-lead glazes.

Materials and context

Ceramics from eleven cities in the Semirechye region and adjacent river valleys, excavated by the Institute of Archaeology of the Republic of Kazakhstan, were analyzed to determine the range of technologies and raw materials employed in glazed ceramic production in the Early Islamic Period. These include the large cities of Aktobe, identified as the site of Balasagun (Shalekenov 2009, p. 52; Akymbek and Baibugunov 2014), Taraz, and Sayram (Isfijab), as well as the smaller trading cities of Akyrtas, Aspara, Bektobe, Kulan, Lower Barskhan, Kastek, Merki, and Tamdy (see Fig. 1). These sites fall into the major river valleys: Sayram along the Arys River which falls in the Syr Darya river valley, Tamdy, Lower Barskhan, Taraz, and Bektobe are in the Talas River valley, Aktobe, Merki, Akrytas, and Aspara in the Chu river valley, and Kastek is on the Kystak river in the Ili river valley.

Geological overview

Southern Kazakhstan is located within the Central Asian Orogenic Belt (CAOB), which is one of the largest orogenic belts in the world (Fig. 2) (Kroner 2015). It covers an area stretching from western Kazakhstan through Kyrgyzstan, Uzbekistan, Tajikistan, and Western China and into eastern Russian. It sits between the Siberian and East European cratons in the north and above the Tarim and North China cratons to the south (Kroner 2015).

The Tianshan (also commonly spelled Tien Shan and Tian Shan) Belt is one of the largest active intracontinental mountain belts in the world (Jepson et al. 2018). The vast mountain system developed throughout the Mesozoic to Cenozoic. The Tianshan region is very complex with multiple major faults, magmatic intrusions, and mountain building events of differing ages (Merkel 2016). The Tianshan is usually divided into three sectors (the Western, Central, and Eastern) and further divided into the North, Middle, and Southern Tianshan based broadly on their regional Paleozoic evolution (Brunet et al. 2017). The distinction between these regions has not been standardized in the literature, and there is a large discrepancy in the terminology between authors following the Russian system and those following the Chinese system. In general, the western and central sectors are divided by the Talas-Fergana Fault, and the Eastern Tianshan (also termed the Chinese Tianshan) lies within China. There is also a discrepancy between what is considered Middle and Northern subdivisions in the former Soviet Republics (predominantly in Kyrgyzstan and Uzbekistan) and in China (Chiaradia et al. 2006).

The Northern Tianshan is situated entirely east of the Talas-Fergana Fault and comprises several Precambrian-age blocks as well as Cambrian-Lower Ordovician ophiolites and marine sediments and is overlain by Ordovician-age sediments and volcanic rocks (Brunet et al. 2017). The Middle Tianshan is separated from the Northern Tianshan by the Terskey suture and comprises a range of Neoproterozoic units which include tillites and acid volcanic rocks (Brunet

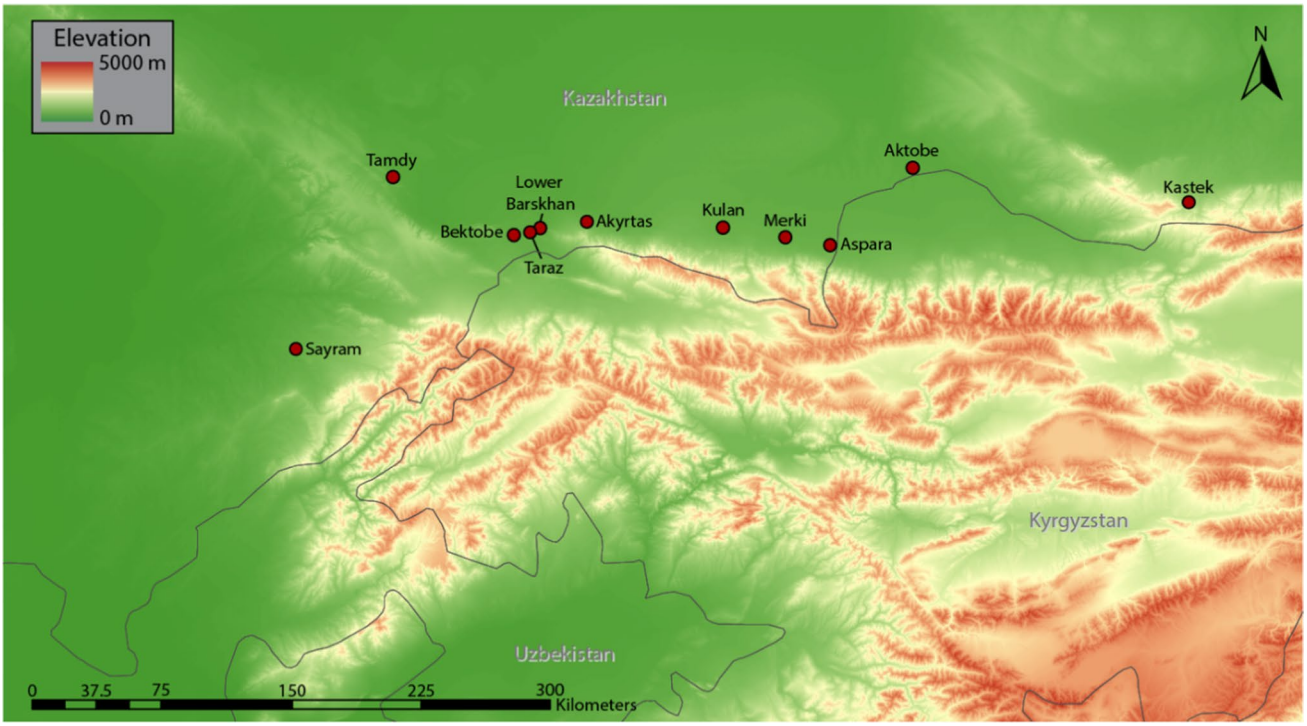

Fig. 1 Location of the eleven sites under study in relation to their modern political borders

et al. 2017). The Southern Tianshan sits along the southern margin of the CAOB. The Southern Tianshan is separated from the Middle Tianshan by the South Tian sutures (also known as the Turestan suture) and is fold-and-thrust belt that is Late Paleozoic in age.

Ten of the eleven sites under study sit to the north/northeast of the Talas-Fergana Fault, where the Northern Tianshan meets the Kazakhstan Terrenes. One site, Sayram, lies west of the Talas-Fergana Fault in the Syr Darya Basin north of the Chatkal Range in the Middle Tianshan region.

Samples

Ninety-five glazed ceramics were selected to create a representative collection of Islamic lead-glazed ceramics from the region. The ceramic sherds were stylistically dated through comparative means to the 9–15th c. CE, although the majority date to the 11–12th c. CE. They were chosen from a larger ceramic assemblage to include representative wares common in the Early Islamic Period, including transparent monochrome ware, splashed ware, underglaze painted ware, underglaze slipped ware, and wide array of opaque wares (Table 1). The majority were uncovered from residential areas, although some were excavated from a ceramic production area at the site of Aktobe. Of the ninety-five ceramics, glaze chemical compositional data for thirty-six were previously published (Klesner et al. 2019).

Thirty-three ceramic sherds from the above collection were chosen for lead isotope analysis to include representative wares common in the Early Islamic Period, including opaque and transparent glazes, as well as to ensure a representative number of ceramics from sites across the region, from the distinct periods under study (9–10th, 11–12th, and 14–15th c. CE), and that were identified as locally produced versus imported based on their paste chemistries (see Table 1 and Fig. 3).

Methods

Chemical compositional analyses

The composition of the glazes was determined by laser ablation-inductively coupled plasma-mass spectrometry (LA-ICP-MS) analysis, which was carried out at the elemental analysis facility (EAF) at the Field Museum of Natural History in Chicago, Illinois. The samples were analyzed with a Thermo ICAP–Q inductively-coupled plasma mass spectrometer connected to a ESI-Elemental Scientific Lasers NW213 laser for direct introduction of solid samples. The methodology follows the standard protocol for glaze and glass analysis employed by the EAF laboratory, which was adapted from Oka et al. (2009) and is described in full in Klesner et al. (2019).

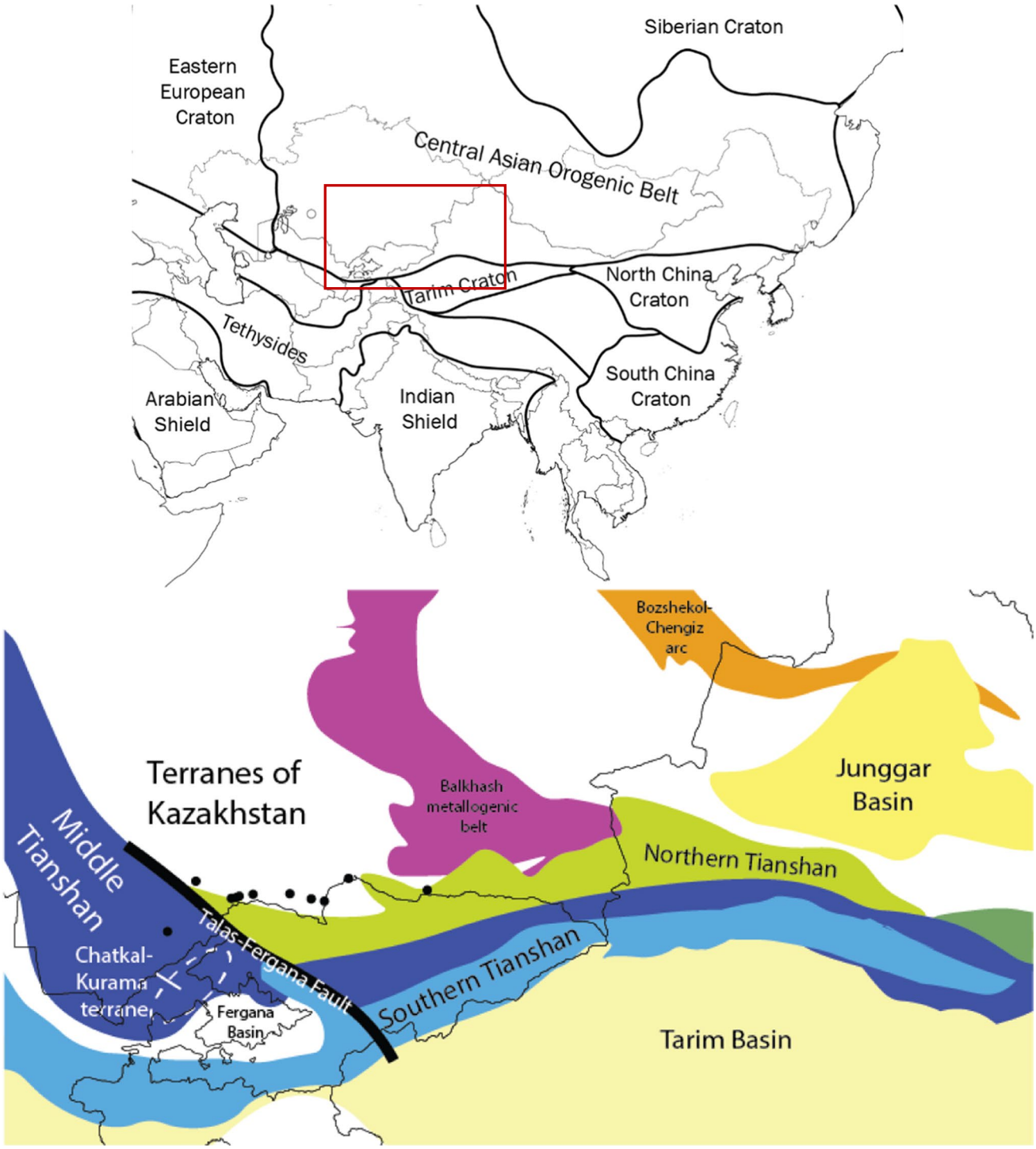

Fig. 2 (*above*) Simplified sketch of tectonic zones on the Asian continent with the region of interest indicated and (*below*) simplified sketch of southwestern section of the CAOB with approximate location of tectonic districts. Black circle represented the location of the sites in this study. Adapted from Alexeiev et al. (2016), Cao et al. (2018), Dolgopolova et al. (2017), Jepson et al. (2018), Shen et al. (2020), and Wang et al. (2020)

Additional compositional information and maps of the distribution of major elements for the glazes were obtained from polished thin-sections and embedded and polished samples using a CAMECA SX100 Ultra electron probe microanalyzer (EPMA) with 5 spectrometers at the Michael J. Drake Electron Microprobe Laboratory at the University

Table 1 Glazed ceramic samples from eleven sites in southern Kazakhstan analyzed in this study

ANID	Site	Date (c. CE)	Paste color	LIA	Glaze type	Slip	Ware	Glaze colors
K007[a]	Lower Barskhan	11–12th	5YR 5/6	x	High-Pb	White	Splashed	Transparent, green, brown
K009[a]	Lower Barskhan	11–12th	5YR 6/6	x	High-Pb w/ Cr	White	Underglaze	Yellow, green, brown
K010[a]	Lower Barskhan	11–12th	5YR 6/4	x	High-Pb Sn-Sb opacified	White	Opaque ware	Green and buff/white
K018[a]	Kulan	11–12th	5YR 5/6		High-Pb	White	Monochrome	Green
K019[a]	Kulan	11–12th	5YR 6/6		High-Pb	White	Monochrome	Green
K020[a]	Kulan	11–12th	2.5YR 6/6		High-Pb	White	Underglaze	Brown and transparent
K027[a]	Aspara	14–15th	10YR 8/4	x	High-Pb w/ Cr	White	Splashed ware	Yellow, green, brown
K028[a]	Aspara	14–15th	7.5YR 7/3	x	High-Pb	White	Monochrome	Green
K029[a]	Aspara	14–15th	10YR 8/1		Sn-opacified Pb Glaze	None	Opaque white	Blue, opaque white
K047[a]	Aktobe	9–10th	5YR 6/6		High-Pb	White	Monochrome	Light yellow
K048[a]	Aktobe	9–10th	5YR 6/6	x	High-Pb	White	Underglaze	Brown and transparent
K049[a]	Aktobe	9–10th	5YR 6/6	x	High-Pb	White	Monochrome	Light yellow
K050[a]	Aktobe	9–10th	5YR 6/6	x	High-Pb	White	Monochrome	Light yellowish/green
K066[a]	Aktobe	11–12th	5YR 6/6	x	High-Pb	White	Monochrome	Transparent
K067[a]	Aktobe	11–12th	5YR 5/6		High-Pb	White	Monochrome	Light yellow
K068[a]	Aktobe	11–12th	5YR 6/6	x	High-Pb	White	Splashed	Green, brown
K069[a]	Aktobe	11–12th	5YR 6/6		High-Pb	White	Underglaze	Black and transparent
K070[a]	Aktobe	11–12th	2.5YR 5/6		High-Pb	White	Underglaze – Incised	Black, gray, and transparent
K071[a]	Aktobe	11–12th	5YR 6/6		High-Pb	White	Underglaze	Light green/blue, reddish brown, black
K072[a]	Aktobe	11–12th	5YR 6/6		High-Pb	White	Underglaze	Brown and transparent
K073[a]	Aktobe	11–12th	5YR 6/6		High-Pb	White	Underglaze	Brown and transparent
K074[a]	Aktobe	11–12th	5YR 5/6		High-Pb	None	Monochrome	Reddish brown
K075[a]	Aktobe	11–12th	2.5YR 6/6		High-Pb	White	Monochrome	Green, black
K076[a]	Aktobe	11–12th	5YR 7/6		High-Pb	White	Underglaze - Incised	Brownish-black and transparent
K077[a]	Aktobe	11–12th	10YR 5/2		High-Pb	White	Monochrome	Olive green
K078[a]	Aktobe	11–12th	7.5YR 6/6		High-Pb	None	Monochrome	Reddish brown
K079[a]	Aktobe	11–12th	5YR 6/6		High-Pb	White	Underglaze	Brown and transparent
K080[a]	Aktobe	11–12th	5YR 7/6		High-Pb	None	Monochrome	Reddish brown
K086[a]	Tamdy	11–12th	7.5YR 6/6		High-Pb	Brown	Monochrome	Reddish brown and transparent
K087[a]	Tamdy	11–12th	5YR 5/6	x	High-Pb	White	Monochrome	Transparent
K088[a]	Tamdy	11–12th	5YR 6/6	x	High-Pb	White	Monochrome	Light yellow
K089[a]	Tamdy	11–12th	5YR 6/6		High-Pb	White	Monochrome	Light green
K090[a]	Tamdy	11–12th	7.5YR 6/6		High-Pb	White	Underglaze	Brown
K099[a]	Bektobe	11–12th	5YR 6/6		High-Pb	White	Underglaze	Brown and transparent
K100[a]	Bektobe	11–12th	7.5YR 7/4		High-Pb	White	Underglaze	Black, brown, and transparent
K106[a]	Kastek	11–12th	5YR 6/6		High-Pb Sb-opacified	White	Splashed	Green
K124	Lower Barskhan	11–12th	5YR 6/6		High-Pb	White	Underglaze	Transparent, dark brown, and reddish brown
K125	Lower Barskhan	11–12th	7.5YR 7/4		High-Pb	White	Underglaze - Incised	Light transparent green and dark green
K126	Lower Barskhan	11–12th	7.5YR 6/6		High-Pb	White	Monochrome	Transparent glaze over white slip
K127	Lower Barskhan	11–12th	5YR 5/4		High-Pb	White	Monochrome	Green
K128	Lower Barskhan	11–12th	2.5YR 6/6	x	High-Pb	Red	Underglaze - Slipped	Brown and reddish-brown

Table 1 (continued)

ANID	Site	Date (c. CE)	Paste color	LIA	Glaze type	Slip	Ware	Glaze colors
K129	Lower Barskhan	11–12th	5YR 6/4	x	High-Pb	White	Underglaze - Incised	Yellowish, red, brown, and transparent
K133	Kulan	11–12th	5YR 6/4		High-Pb	White	Monochrome	Transparent
K134	Kulan	11–12th	5YR 6/4		High-Pb	White	Underglaze	Yellow, brown, and transparent
K135	Kulan	11–12th	7.5YR 4/3		High-Pb	White	Monochrome	Transparent
K136	Kulan	11–12th	5YR 6/6		High-Pb Sn-opacified	White	Monochrome opaque	Opaque white
K142	Tamdy	11–12th	5YR 7/3	x	High-Pb w/ Cr	White	Underglaze	Green, yellow, brown, reddish-orange, and transparent
K143	Tamdy	11–12th	2.5YR 5/6		High-Pb	White	Monochrome	Light green transparent
K144	Tamdy	11–12th	2.5YR 6/6		High-Pb	White	Monochrome	Transparent
K145	Tamdy	11–12th	2.5YR 7/4		High-Pb	White	Monochrome	Transparent
K146	Tamdy	11–12th	2.5YR 7/6		High-Pb	White	Monochrome	Green
K149	Bektobe	11–12th	5YR 6/6	x	High-Pb	White	Underglaze—Calligraphy	Transparent and brown
K150	Bektobe	11–12th	5YR 6/4		High-Pb	White	Monochrome	Transparent
K151	Bektobe	11–12th	2.5YR 6/8		High-Pb	White	Underglaze	Transparent and brown
K152	Bektobe	11–12th	5YR 6/6	x	Low-lead (4 wt% PbO)	White	Monochrome	Light green transparent
K153	Bektobe	11–12th	5YR 6/6		High-Pb	White	Monochrome	Light green and transparent
K154	Bektobe	11–12th	7.5YR 8/4		Alkali (high Mg + Ca)	White	Monochrome	Transparent
K155	Bektobe	11–12th	5YR 6/6		High-Pb	White	Monochrome	Light green transparent
K156	Bektobe	11–12th	5YR 6/8	x	High-Pb	White	Underglaze	Green
K166	Merki	11–12th	7.5YR 7/3		High-Pb	White	Monochrome	Transparent
K167	Merki	11–12th	2.5YR 6/4		Burnished slip	Red	Burnished slip	Very thin reddish-brown burnished slip
K168	Merki	11–12th	5YR 6/4	x	High-Pb	White	Monochrome	Light green transparent
K169	Merki	11–12th	2.5YR 6/6	x	High-Pb	White	Underglaze – Calligraphy	Brown and transparent
K170	Merki	11–12th	7.5YR 7/4		High-Pb	White	Monochrome	Transparent
K171	Merki	11–12th	5YR 7/4	x	High-Pb	White	Monochrome	Transparent
K175	Taraz	10–12th	2.5YR 6/6	x	High-Pb w/ Cr	White	Underglaze—yellow staining?	Yellow with olive-green
K176	Taraz	10–12th	5YR 5/6		High-Pb w/ Cr	White	Underglaze—yellow staining?	Yellow and brown
K177	Taraz	10–12th	7.5YR 7/4	x	High-Pb	White	Underglaze - Incised	Transparent
K178	Taraz	10–12th	5YR 7/6		High-Pb Sb-opacified	White	Opaque ware	White, brown, and red
K179	Taraz	10–12th	10YR 7/4	x	High-Pb	none	Underglaze?	Green
K180	Taraz	10–12th	5YR 6/6		High-Pb	White	Monochrome	Transparent
K181	Taraz	10–12th	5YR 6/6		High-Pb w/ Cr	White	Underglaze—yellow staining or olive	Yellow, olive-green, and brown
K182	Taraz	10–12th	5YR 7/6		High-Pb	White	Underglaze	Transparent, dark brown, and reddish-brown
K183	Taraz	10–12th	5YR 5/6	x	High-Pb w/ Cr	White	Underglaze—yellow staining?	Yellow and olive-green
K184	Taraz	10–12th	5YR 7/4	x	High-Pb	White	Monochrome	Light transparent green
K185	Taraz	10–12th	5YR 6/6		High-Pb Sn- and Sb-opacified	White	Opaque, underglaze?	Green and brown
K186	Taraz	10–12th	5YR 7/6		High-Pb	White	Underglaze	Transparent and brown
K192	Akyrtas	11–12th	2.5YR 6/6	x	High-Pb	White	Monochrome	Transparent
K193	Akyrtas	11–12th	2.5YR 6/8		High-Pb	White	Monochrome	Green

Table 1 (continued)

ANID	Site	Date (c. CE)	Paste color	LIA	Glaze type	Slip	Ware	Glaze colors
K194	Akyrtas	11–12th	5YR 6/6		High-Pb	White	Monochrome	Transparent
K195	Akyrtas	11–12th	2.5YR 6/6	x	High-Pb	White	Monochrome	Transparent
K196	Akyrtas	11–12th	5YR 6/6		High-Pb Sb-opacified	White	Monochrome opaque	Yellow
K198	Aktobe–Kiln	10–12th	2.5YR 5/8	x	High-Pb	White	Monochrome	Light yellow
K199	Aktobe–Kiln	10–12th	10R 4/1	x	High-Pb	White	Underglaze	Brown
K200	Aktobe–Kiln	10–12th	2.5YR 5/1	x	High-Pb	White	Monochrome	Transparent
K201	Aktobe–Kiln	10–12th	2.5YR 5/4		High-Pb	White	Underglaze	Transparent and brown
K202	Aktobe–Kiln	10–12th	5YR 6/8		High-Pb	White	Underglaze	Transparent and reddish-brown
K203	Aktobe–Kiln	10–12th	2.5YR 5/2		High-Pb	White	Underglaze	Transparent and brown
K205	Sayram	9th	7.5YR 7/4	x	High-Pb Sn- and Sb-opacified, and Pb-alkali Sn-opacified	none	Green and white opaque	Green and opaque white
K206	Bektobe	11–12th	5YR 6/6		High-Pb	White	Underglaze	Black and transparent
K207	Bektobe	11–12th	5YR 7/4		High-Pb	White	Underglaze	Transparent
K210	Lower Barskhan	11–12th	2.5YR 6/6		High-Pb	White	Monochrome	Light green, yellow, and brown
K211	Lower Barskhan	11–12th	2.5YR 6/6		High-Pb	White	Monochrome	Light green transparent
K212	Lower Barskhan	11–12th	2.5YR 5/6	x	High-Pb Sn- and Sb-opacified	White	Monochrome opaque	Opaque yellow
K213	Lower Barskhan	11–12th	5YR 6/4		High-Pb Sb-opacified	White	Monochrome opaque	Opaque light yellow

[a]Glaze compositional data published in Klesner et al. (2019)

of Arizona. Instrumental parameters included an accelerating voltage of 15 keV, 8 nA for alkalis (Na and K), which were counted first, and 40 nA for all other elements, and a spot size of 1 or 10 µm. Wavelength-dispersive spectroscopy (WDS) data was obtained for 17 elements: Na, Mg, Al, Si, P, K, Ca, Ti, Cr, Mn, Fe, Co, Cu, Mo, Sn, Sb, and Pb. The elements were calibrated with standards chosen and maintained by K. Dominik, and the microprobe methodology is described in full in Klesner et al. (2021).

LIA

Minimally destructive sampling of the lead glazes was undertaken for this research. For high-lead materials, such as lead metal and galena, lead sampling using swabs is well established (Thibodeau et al. 2012). Additionally, research by Santarelli (2015) has demonstrated that sampling by swabbing was also feasible for high-lead glazes. The minimally destructive swabbing method was chosen for this analysis for two reasons. First, it is more cost effective and requires less laboratory time than the destructive digestion method usually employed for isotope analysis of lead glazes. Secondly, the physical properties of the Islamic lead glazes under study benefit from only analyzing the surface of the glaze.

The swabbing methodology utilized in this research is adapted from Santarelli (2015). The sampling of the lead glazes was done using a cleanroom laundered polyester-tipped swab (CleanTips® Polyester Alpha® Mini Swab, ITW Texwipe®). Initially, a swab dipped in twice-distilled 2% HNO_3 was used to clean the sampling surface of the glaze to remove any dirt particles or contaminants from the surface. A second swab was then dipped in a second, clean vial of twice-distilled 2% HNO_3, and the surface of the glaze was swabbed for approximately 1 min. The swab was stored in a Falcon tube and soaked in 1 ml of twice-distilled 2% HNO_3 for 2 h. The solution was then transferred to a PFA Savillex® vial where it was evaporated.

The lead extraction followed the standard procedure used for lead isotope analysis at the University of Arizona (Thibodeau et al. 2012; Santarelli 2015) or following the ion exchange chromatography protocol used at MURR and adapted from Weis et al. (2006). The lead isotope analysis was conducted on the Nu Plasma II (Nu Instruments) multi collector-inductively coupled plasma-mass spectrometer (ICP-MS) at MURR. Most samples ($n = 23$) were introduced to the instrument in wet plasma, and a few samples, presenting lower lead amount ($n = 10$), were introduced using a Desolvating Nebulizer (DSN-100, Nu Instruments). All lead dry residues were dissolved in 0.5 ml 14 N HNO_3, evaporated at 90 °C, and finally re-digested in 0.05 N HNO_3 Optima prior to analysis on the Nu Plasma II. The instrument was optimized to obtain about 100 mV and 150 mV at mass 204 in wet and dry plasma respectively. Standard and

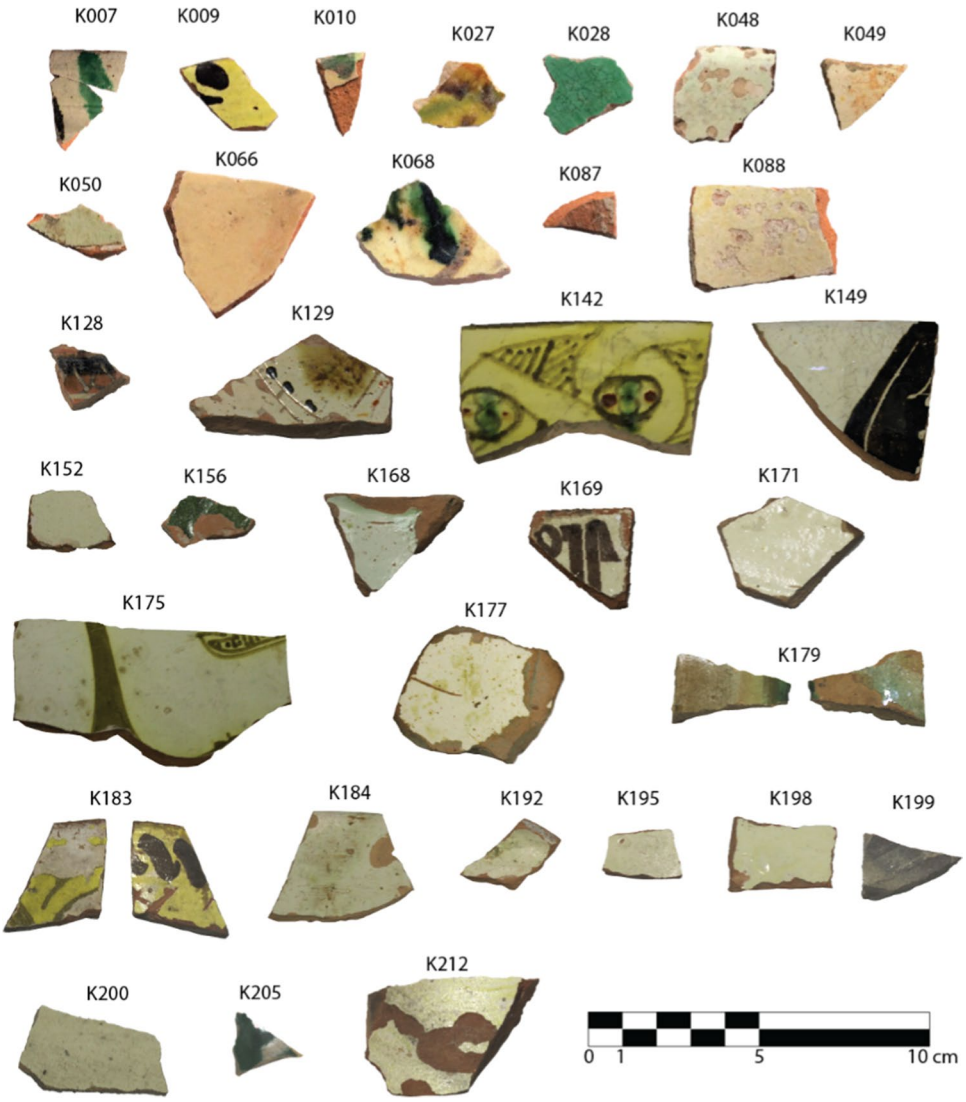

Fig. 3 Glazed ceramics analyzed by lead isotope analysis from Lower Barskhan (K007, K008, K010, K128, K129, and K212), Aspara (K027–K028), Tamdy (K087–K088, K142), Bektobe (K149, K152, K156), Merki (K168, K169, K171), Taraz (K177, K179, K183, K184), Akyrtas (K192**,** K195), Sayram (K205), and Aktobe, from the town (K048, K049, K050, K066, and K068) and from the ceramic production area (K198–K200)

sample solutions were spiked with the Tl standard reference material SRM997 to obtain a Pb/Tl of ~ 4. All sample solutions were prepared to obtain a concentration matching that of the standard solution (SRM981) of about 150 ppb Pb in wet and 30 ppb in dry plasma. The standard was run multiple times at the beginning of each session and after every two samples. Sample and standard measurements were corrected for mass fractionation using the NIST value for Tl ratio ($^{205}Tl/^{203}Tl = 2.38714$) and mass interference of mercury at mass 204 using the value of 0.229883 for $^{204}Hg/^{202}Hg$ natural ratio. Average values ($n = 56$) obtained for the SRM981 in wet plasma were 36.689 ± 0.007 (2SD) for $^{208}Pb/^{204}Pb$, 15.489 ± 0.002 (2SD) for $^{207}Pb/^{204}Pb$, and 16.936 ± 0.002 (2SD) for $^{206}Pb/^{204}Pb$, respectively. Average values ($n = 17$) obtained for the SRM981 in dry plasma were 36.677 ± 0.005 (2SD) for $^{208}Pb/^{204}Pb$, 15.484 ± 0.001 (2SD) for $^{207}Pb/^{204}Pb$, and 16.933 ± 0.002 (2SD) for $^{206}Pb/^{204}Pb$, respectively. These values are in agreement with long-term values obtained on the Nu Plasma II at MURR. Sample values were additionally corrected by standard bracketing (see Weis et al. 2006) using recommended values from Galer and Abouchami (1998). Three replicates (i.e., second analysis of the same solutions) were measured (two in wet plasma, one in dry plasma), and one replicate was run both in wet and dry plasma (Table 5) to evaluate the reproducibility of the analyses.

Results

Compositional analysis

Glaze recipes

Several distinct glaze types were identified for the sherds included in this study, including alkali-fluxed glaze, low-lead

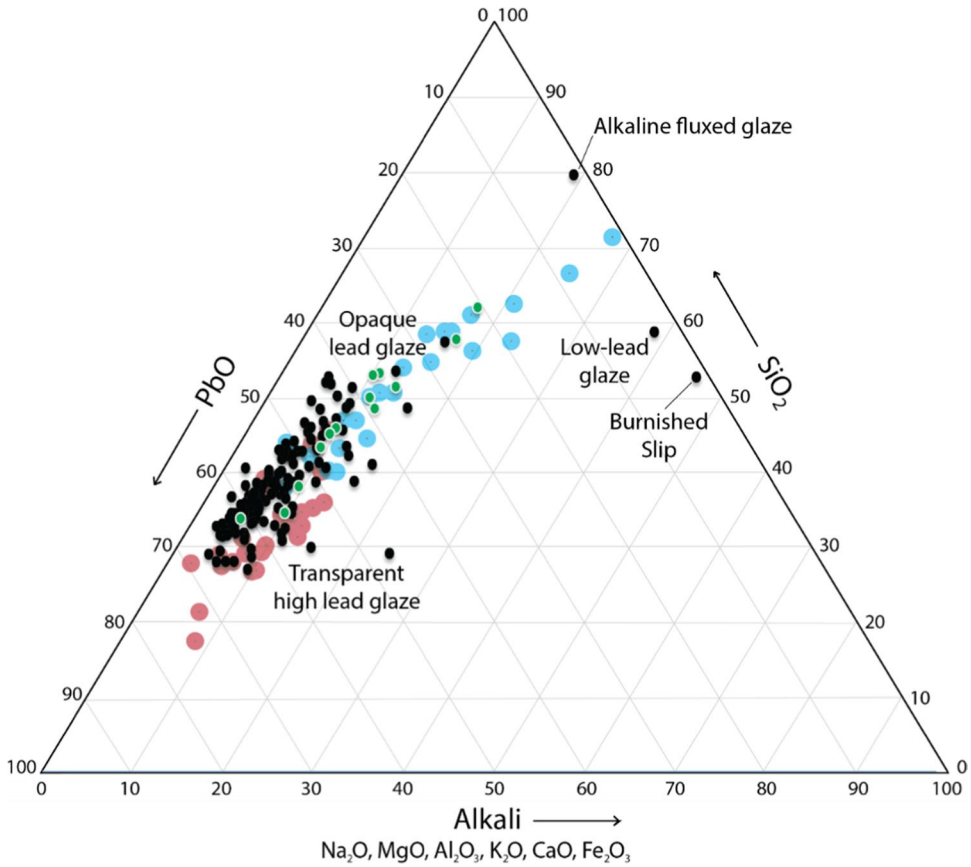

Fig. 4 Ternary diagram showing the major chemical compositions for the alkaline-fluxed glaze, alkali-lead glaze, low-lead glaze, opacified lead glaze, and traditional high-lead glazes for the 104 glazed ceramics in this study. All samples are indicated with a black circle, except for the opacified glazes (green circle). Concentrations are in oxide weight percent compared to transparent high-lead glazes (red circle) and tin-opacified glazes (blue circle) compositions reported in Tite et al. (1998). Figure is adapted from Klesner et al. (2019)

glaze (PbO ~ 4 wt%), and transparent and opacified high-lead glaze (PbO > 35 wt%) (Fig. 4). There was also one sample that was not glazed but had a highly burnished slip. Average compositions for these glaze types can been see in Table 2 and Table 3. The majority of samples (80%) had a traditional transparent high-lead glaze, with an average composition of 54.04 wt% PbO, 37.61 wt% SiO_2, and 3.16 wt% Al_2O_3, and the alkali content ($Na_2O + K_2O$) was less than 2 wt% (Table 2). This is comparable to the compositions of the standard high-lead glaze produced throughout the Islamic, Byzantine, and Medieval European world as reported by Tite et al. (1998). It is also very similar to the composition of the 9–11th c. transparent lead glazes from Termez reported by Molera et al. (2020), which had an average compositions of 53.7 wt% PbO, 39.8 wt% SiO_2, 2.7 wt% Al_2O_3, and 1.9 wt% total alkali.

The transparent high-lead glazes are very uniform in their composition when colorants are removed from analysis. This is best demonstrated through a principal component analysis[1] (PCA) of the transparent high-lead glazes (n = 126 analyses on 66 sherds). The PCA for 50 elements (all elements excluding Au and W and those associated with colorants: Co, Cu, Fe, Mn, Cr) indicates that the first eleven principal components explained over 90% of the total variance (see Supplementary Information). The transparent lead glazes behave as a single group (Fig. 5) and no differentiation observed between glazes of different periods of production, provenance, or ware for any of the transparent high-lead glazes across the first eleven principal components. This confirms the results of the preliminary study that the samples are not differentiable by the major, minor, or trace element concentrations in the glazes (Klesner et al. 2019).

Three unique glaze recipes were identified (Table 2). One sample, K154, had a glaze fluxed with MgO and CaO in high concentrations (23.07 and 16.62 wt% respectively) and 5.76 wt% TiO_2 in the glaze. K152 has a much lower PbO concentration of (3.94 wt%) compared to the traditional high-lead glazes (45–60 wt%). Its total alkali concentration is 4.36 wt% and has a large amount of Al_2O_3 (21.16 wt%). The final unique surface coating observed in the collection is sample K167, which has a burnished red slip (2.5YR 6/4). The slip is composed of 4.64 wt% Fe_2O_3, 19.99 wt% Al_2O_3, 58.32 wt% SiO_2, and 7.45 wt%

[1] PCA is a pattern recognition technique often used to investigate archaeological datasets. One of the strengths of PCA is that it can simultaneously display both variables (measured elements) and objects (individual analyzed samples) on the sample set of principal component reference axes. This is discussed by Baxter (1992), Baxter and Buck (2000), and Neff (1994, 2002).

Table 2 Bulk composition of glaze types identified in this analysis as determined by LA-ICP-MS. Only elements significant in the identification of glaze types are reported below. See Supplementary Information for full results

Oxide (reported in wt% unless noted)	Transparent high-lead glaze						Alkali-fluxed glaze	Low lead glaze	Burnished slip
	Samples = 66 (126 total analyses)						$n = 1$ (K154)	$n = 1$ (K152)	$n = 1$ (K167)
	Mean		σ	Range					
SiO_2	37.61	±	5.73	26.79	-	52.35	49.31	58.21	58.32
Na_2O	0.28	±	0.17	0.03	-	0.91	0.40	0.78	1.12
MgO	0.51	±	0.24	0.11	-	1.30	23.07	2.34	1.92
Al_2O_3	3.16	±	1.01	1.19	-	7.95	2.19	21.16	19.99
P_2O_5	0.14	±	0.11	< 0.01	-	0.70	0.12	0.15	0.40
Cl	0.09	±	0.20	0.01	-	1.67	0.34	0.02	1.76
K_2O	0.91	±	0.65	0.17	-	4.70	0.40	3.59	6.33
CaO	1.15	±	0.60	0.32	-	3.30	16.62	4.65	5.32
MnO	0.27	±	0.64	< 0.01	-	3.84	0.03	0.11	0.04
Fe_2O_3	1.32	±	2.20	0.15	-	18.69	1.65	4.97	4.64
CuO	0.56	±	1.51	0.01	-	10.25	0.11	0.01	< 0.01
SnO_2	0.01	±	0.03	< 0.01	-	0.19	< 0.01	< 0.01	< 0.01
PbO	54.04	±	6.77	38.70	-	65.95	0.02	3.94	0.01
TiO_2	0.12	±	0.06	0.02	-	0.43	5.76	0.46	0.46
Sb (ppm)	242.9	±	414.5	5.0	-	2298.6	13.7	4.1	2.7

Table 3 Composition of the opacified glaze samples as determined by LA-ICP-MS. Only elements significant in the identification of glaze types are reported below. See Supplementary Information for full results

Oxide (reported in wt% unless noted)	Tin-opacified glaze						Tin- and antimony-opacified glaze						Antimony-opacified glaze					
	Samples = 2 (3 total analyses)						Samples = 4 (7 total analyses)						Samples = 4 (6 total analyses)					
	Mean		σ	Range			Mean		σ	Range			Mean		σ	Range		
SiO_2	46.21	±	1.75	44.80	-	48.17	46.80	±	11.34	34.09	-	61.56	46.94	±	5.87	37.00	-	52.54
Na_2O	2.59	±	1.91	0.38	-	3.70	1.33	±	1.97	0.15	-	5.42	0.40	±	0.26	0.17	-	0.73
MgO	0.72	±	0.27	0.42	-	0.95	0.84	±	0.30	0.54	-	1.32	0.63	±	0.40	0.31	-	1.33
Al_2O_3	3.99	±	4.81	1.18	-	9.54	5.07	±	2.81	2.20	-	9.76	4.13	±	1.28	2.10	-	5.63
P_2O_5	0.12	±	0.04	0.08	-	0.15	0.30	±	0.27	0.13	-	0.89	0.25	±	0.17	0.13	-	0.59
Cl	0.06	±	0.01	0.05	-	0.08	0.07	±	0.03	0.04	-	0.11	0.07	±	0.09	0.02	-	0.25
K_2O	1.39	±	0.47	1.00	-	1.91	2.19	±	1.40	0.43	-	4.11	1.27	±	0.59	0.50	-	2.01
CaO	1.44	±	0.94	0.37	-	2.05	1.62	±	0.86	0.43	-	2.38	2.66	±	0.95	1.40	-	3.80
MnO	0.02	±	0.01	0.01	-	0.03	0.18	±	0.33	0.01	-	0.93	0.04	±	0.06	0.01	-	0.16
Fe_2O_3	0.84	±	0.31	0.53	-	1.15	0.88	±	0.79	0.35	-	2.54	1.68	±	2.22	0.39	-	6.14
CuO	0.26	±	0.22	0.00	-	0.40	1.64	±	2.52	0.04	-	6.45	0.48	±	0.72	0.03	-	1.93
SnO_2	7.06	±	4.64	1.69	-	9.76	0.97	±	1.04	0.35	-	3.28	0.03	±	0.03	0.00	-	0.06
PbO	35.45	±	1.49	33.82	-	36.75	37.72	±	15.20	16.27	-	58.96	40.59	±	8.09	33.55	-	54.53
Sb_2O_5	0.01	±	0.02	0.00	-	0.04	0.21	±	0.13	0.02	-	0.38	0.59	±	0.56	0.25	-	1.67
Co (ppm)	2099.6	±	3618.1	2.5	-	6277.4	3.2	±	2.0	1.0	-	6.3	2.5	±	1.2	1.2	-	4.3
Pb/Sn	11.34	±	12.34	4.10	-	25.58	79.65	±	49.04	5.85	-	162.8						
Pb/Sb					-		307.91	±	312.75	110.98	-	998.01	127.2	±	59.1	33	-	202

total alkali content, with its red color resulting from the oxidized iron in the slip. Burnished slips were common in Central Asia, especially in Transoxiana beginning in the Hellenistic period (Puschnigg and Houal 2019) and were

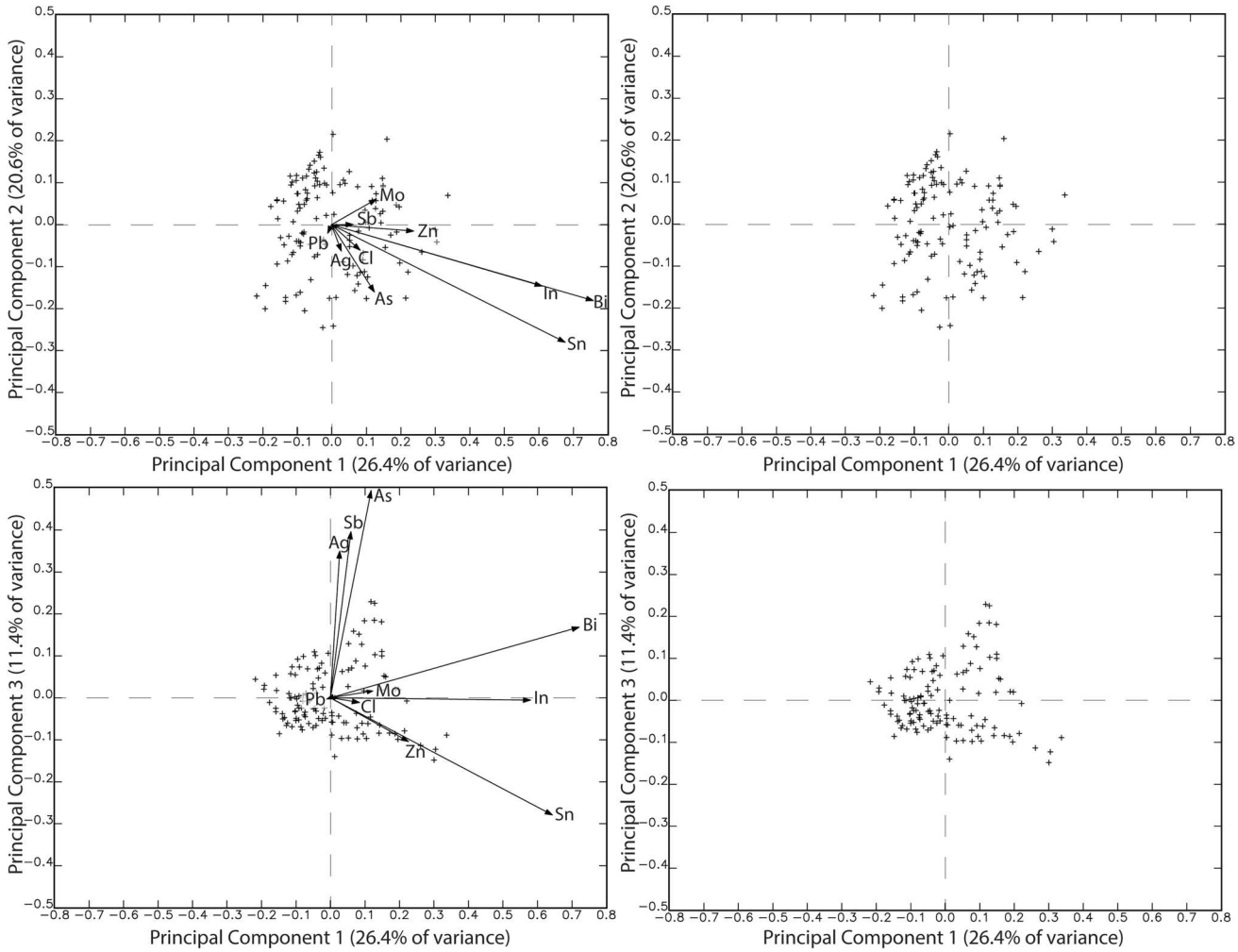

Fig. 5 (*top*) Biplots of principal component 1 (26.4% of total variance) versus principal component 2 (20.6% of total variance) and (*bottom*) principal component 1 versus principal component 3 (11.4% of total variance) for the transparent high-lead glazes analyzed by LA-ICP-MS. Only the nine elements with the largest contribution to variation, and lead, are indicated

still produced in the Islamic period, particularly in the regions of Ferghana and Chach in Transoxiana.[2]

Opacified ceramics

Ten of the ceramics in this study have an opaque glaze. These ceramics fall into three categories: (1) tin-opacified, (2) tin- and antimony-opacified, and (3) antimony-opacified (see Fig. 6 and Table 3). Their overall composition is similar, with the average PbO concentration ranging from 35.45 to 40.59 wt% and SiO_2 ranging from 46.21 to 46.94 wt%.

Two samples have a tin-opacified glaze. K029, which dates from the 14–15th c. CE, has a Pb/Sn ratio of 4, and total alkali content is 4.81 wt%, which corresponds to the majority of opaque Islamic white glazed wares produced in the Medieval Period (Matin 2019). The glaze has a high amount of total opacifier, averaging 9.74 wt% SnO_2. The distribution of the SnO_2 particles can be seen in Fig. 7. This sherd has a white (10YR 8/1) fritware body. Fritware was new ceramic ware that was developed in the 11th c. CE in Egypt and spread east to Iran in the 12th c. CE, where its production flourished (Watson 2020). It is characterized as having a white, sandy body that is composed of quartz, glass frit, and white clay (Allan 1991, p. 16). The only examples of fritware in this collection are from the 14–15th c., which is to be expected as the fritware body becomes the predominant ware for fine glazed wares in Central Asia by the 13th c. (Watson 2004, p. 41). The other tin-opacified glaze sample,

[2] Burnished red slips are discussed in the "Central Asia" article in (2009) Bloom, J., & Blair, S. (Eds.), The Grove Encyclopedia of Islamic Art and Architecture. Oxford University Press. Pg 421.

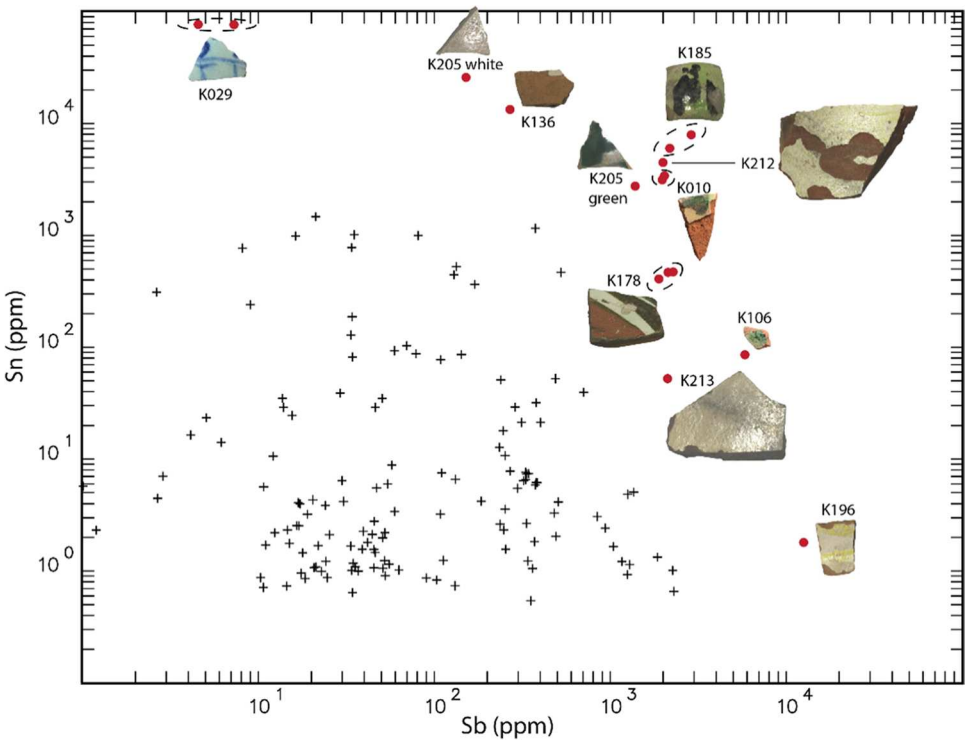

Fig. 6 A scatterplot of Sb versus Sn concentrations (in ppm – log base 10 scale) for the glazed ceramics, with the opaque glazes (red circle) indicated. The opaque ceramics include Sn-opacified glazes (K029, K136, and K205 white), Sn- and Sb-opacified glaze (K010, K185, K205 green, and K212), and Sb-opacified glazes (K106, K178, K196, and K213)

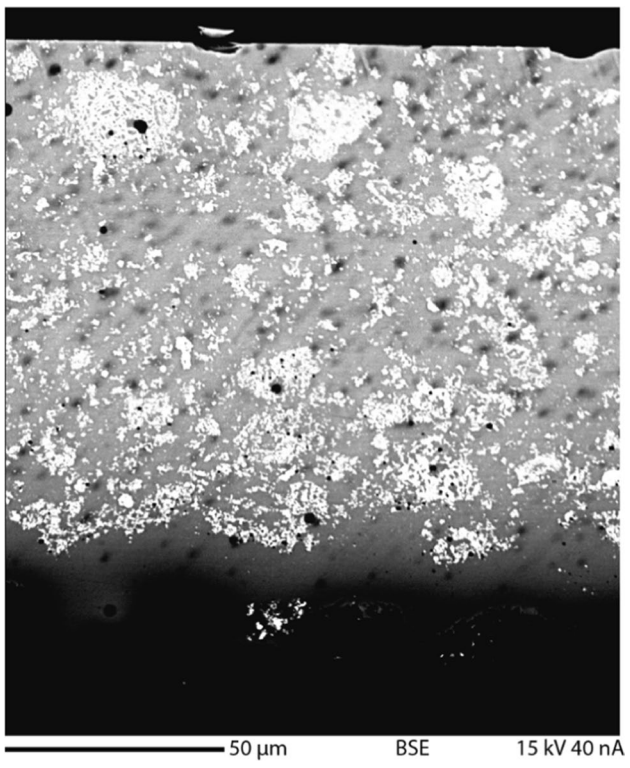

Fig. 7 Backscattered electron (BSE) image of the opaque white glaze on K029 showing the distribution of Sn-oxide particles. The Sn-oxide particles appear white because of higher average atomic number

K136, has a much lower concentration of SnO_2 (1.69 wt%) but is still in high enough concentrations to be a deliberate addition to the glaze and for SnO_2 particles to remain undissolved in the glaze matrix (Tite 2011).

Four of the samples (K010, K185, K205, and K212) have significant concentrations of both tin (generally > 1 wt%) and antimony (generally > 0.2 wt%) in the glaze and are thus categorized as having a tin- and antimony-opacified glaze (Table 3). K010 and K212 have less than 1 wt% SnO_2 in the glaze as measured by LA-ICP-MS (0.43 and 0.57 wt%, respectively) but have visible SnO_2 particles in the glaze matrix, while K205 has slightly less than 0.2 wt% Sb_2O_5 (0.18 wt%) but again has visible antimony in the particles of the glaze and are thus included in this category. K212 has an opaque pale-yellow glaze (5Y 8/4), is thin, and varies in thickness from 10 to 50 µm. Distributed throughout the glaze are micron and sub-micron-sized particles that are composed of Sb_2O_5 and SnO_2 (Fig. 8), with an average ratio of 1:2, respectively. The distribution of the particles is not uniform, with clusters of particles observed. A similar phenomenon was documented by Shortland (2002) in the analysis of 2nd millennium BCE Egyptian yellow glass opacified with lead antimonate.

K205, which dates to the 9th c. and was recovered at the site of Sayram, has two distinct glaze compositions. On the interior surface, it has a green and white high-lead opacified glaze (48.43 wt% PbO), while the exterior has a white opacified glaze which has a much lower concentration of PbO (16.27 wt%) and is classified as a lead-alkali

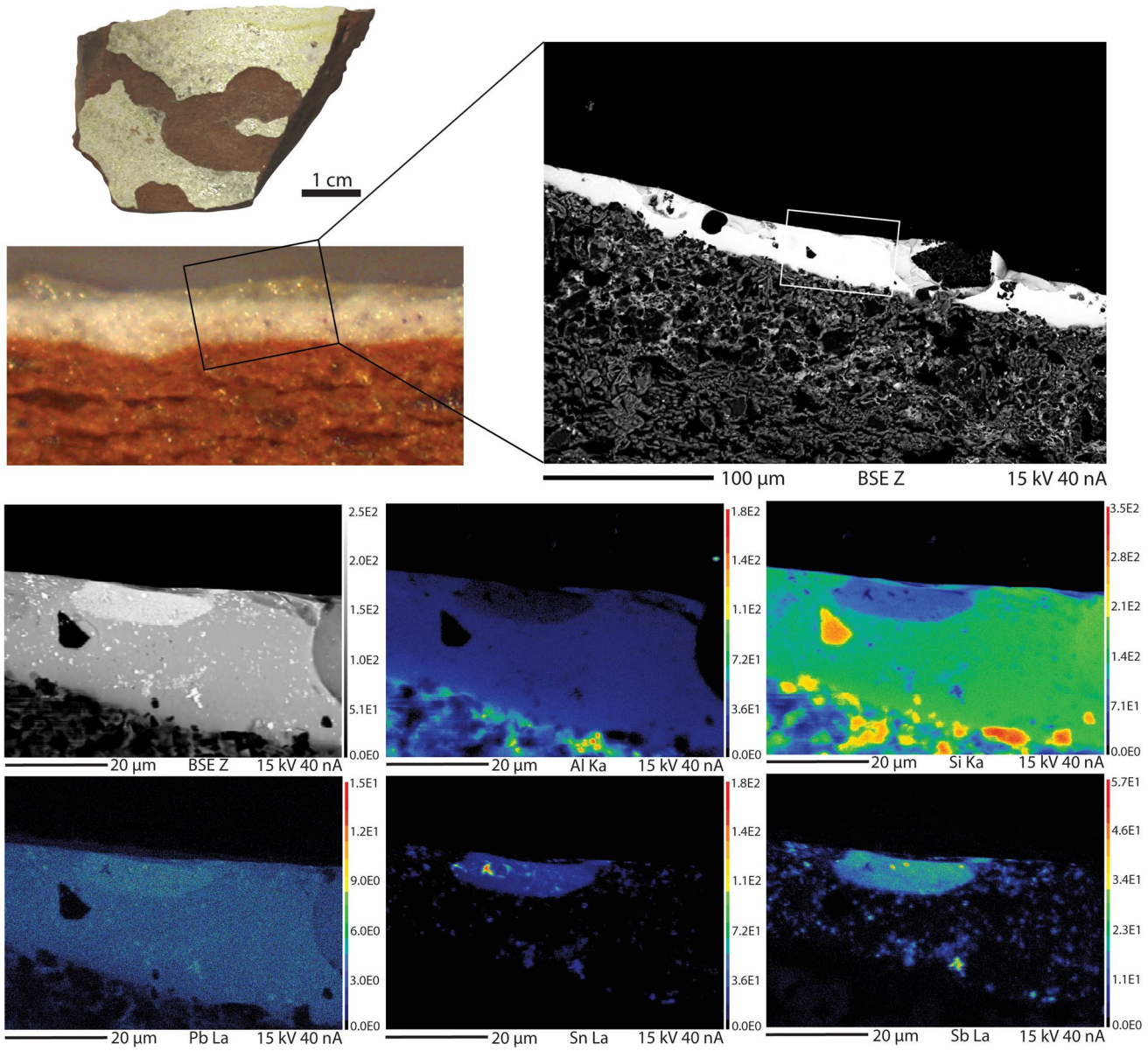

Fig. 8 Electron microprobe elemental maps of the opaque yellow glaze on K212 showing the distribution of Al, Si, Sb, Sn, and Pb in the glaze and slip of the sample. Scale bar represents 20 µm. The white boxes on the BSE image indicate the mapped region. Adapted from Klesner et al. (2021)

glaze. The different glaze types on K205 can be seen in Fig. 9. The tin- and antimony-oxide particles are the opacifying agents in the green glaze, with antimony distributed in the predominantly SnO_2 particles (Fig. 9), while SnO_2 and undissolved quartz particles are the opacifiers in the white glaze.

K185 and K010 both have multiple glaze colors that were analyzed. For K185, the green and black glazes had the same ratio of Sb_2O_5:SnO_2 (0.38), indicating that the opacifier is independent of the colorants used in the glaze recipes. K010 similarly had a ratio of 0.62 Sb_2O_5:SnO_2 for its green glaze and 0.66 for the white/buff color, which again suggests that the opacifier is independent of the glaze colorant for these samples.

Four samples, K106, K213, K196, and K178, have an antimony based opacifier. The glaze colors on these samples include yellow, green, white, brown, and red. The range of

Fig. 9 *(Above)* Electron microprobe elemental mapping of the opaque green glaze on K205 showing the distribution of Al, Si, Pb, Sn, and Sb in the glaze. (*Below*) Electron microprobe elemental mapping of the opaque white glaze on K205 showing the distribution of Al, Si, Pb, Na, and Sn in the glaze. The white boxes on the BSE image indicate the mapped region

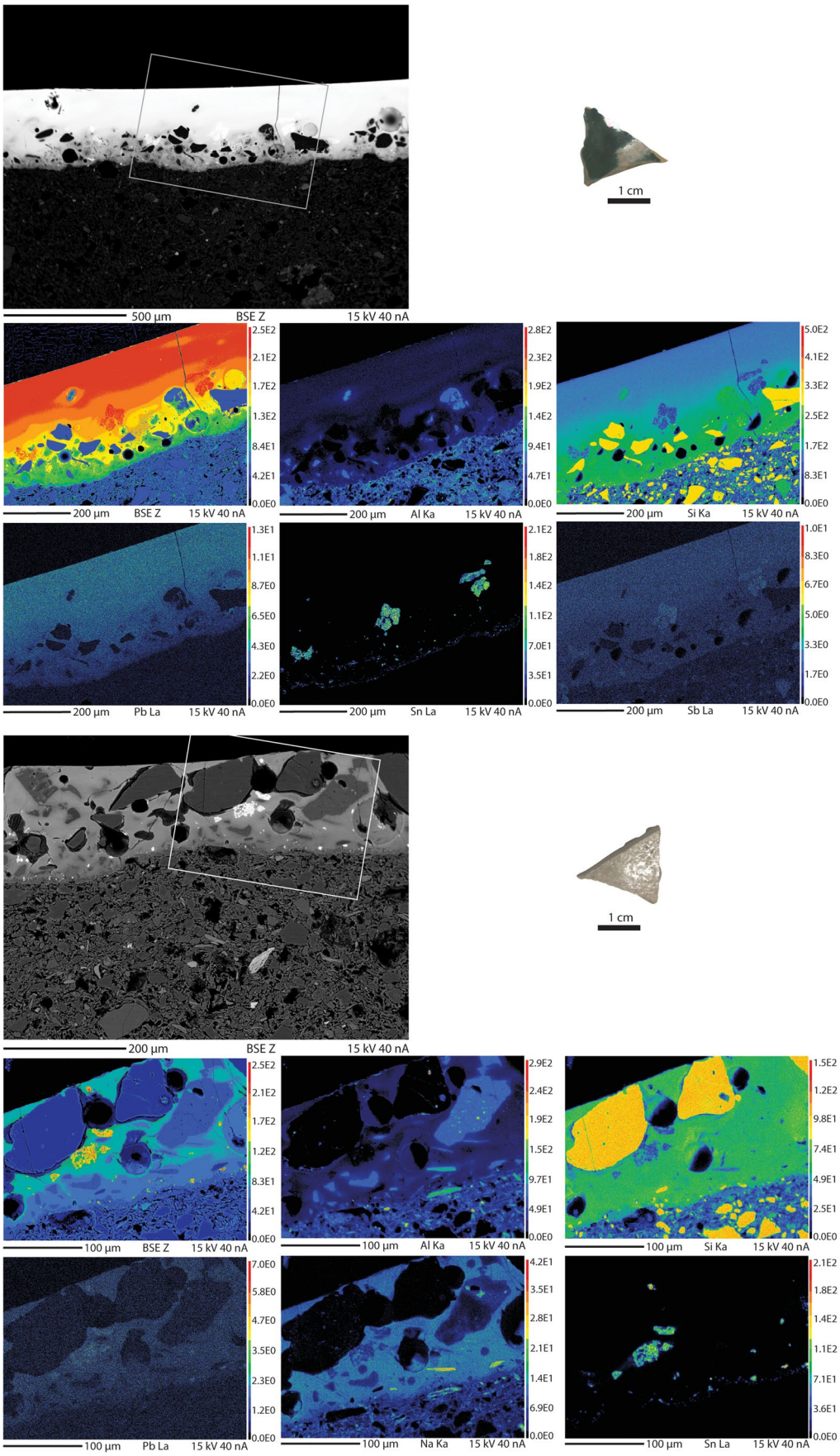
500 µm BSE Z 15 kV 40 nA
1 cm
200 µm BSE Z 15 kV 40 nA
200 µm Al Ka 15 kV 40 nA
200 µm Si Ka 15 kV 40 nA
200 µm Pb La 15 kV 40 nA
200 µm Sn La 15 kV 40 nA
200 µm Sb La 15 kV 40 nA
200 µm BSE Z 15 kV 40 nA
1 cm
100 µm BSE Z 15 kV 40 nA
100 µm Al Ka 15 kV 40 nA
100 µm Si Ka 15 kV 40 nA
100 µm Pb La 15 kV 40 nA
100 µm Na Ka 15 kV 40 nA
100 µm Sn La 15 kV 40 nA

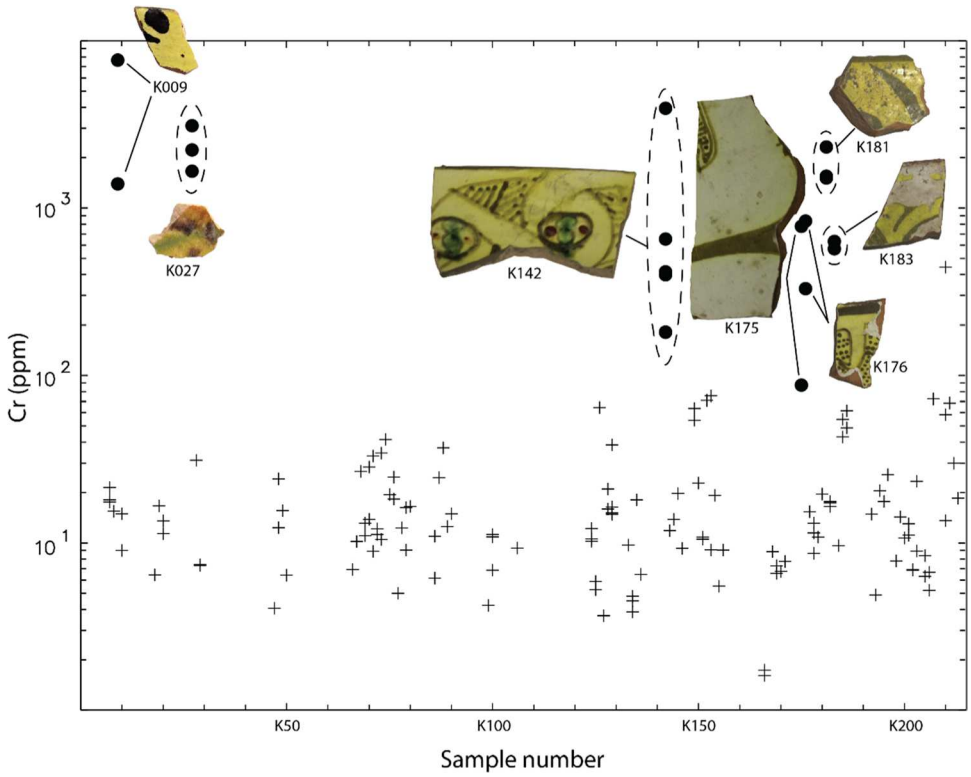

Fig. 10 A displaying Cr concentrations (in ppm – log base 10 scale) for the glazed ceramics, with the glazes high in Cr (black circle) indicated

Sb_2O_5 found in the glaze (0.25–1.67 wt%) is comparable to antimony-opacified glazed from the 9–11th c. CE Egypt (0.1–1.9 wt% Sb_2O_5) as measured by Salinas et al. (2019). Identification of the mineral phases of the Sb-rich particles will require the use of X-ray diffraction or Raman spectroscopy, but the opaque yellow color present in the antimony based–opacified glazes suggests that it is in the form of lead antimonate ($Pb_2Sb_2O_7$).

Colorants

Cobalt, copper, chromium, manganese, and iron were observed as colorants in these ceramics. A cobalt blue glaze is observed on K029, and the sherd dates to the 14–15th c. CE. Only a very small amount of cobalt is needed to impart color, and the concentration was 0.80 wt% CoO. Copper green is the most common colorant, with 16 samples having over 1 wt% CuO in the glaze. The average concentration of CuO is 4.05 wt% but was recorded up to 10.25 wt%. Copper was also seen on the widest variety of glaze types, including high-lead glaze, tin- and antimony-opacified glaze, and antimony-opacified glaze. Manganese colorants were used to create brown and black glazes. Twenty samples had significant concentrations of MnO, and the average concentration was 1.53 wt%. MnO in the presence of high-lead glazes can produce a brown-, black-, or purple-colored glaze. Manganese, however, only forms a purple glaze when it is in the glass phase in the form of manganese ions (Mn^{3+}) (Tite 2011; Molera et al. 2013), which is not observed in these samples.

Seven samples have significant concentrations of Cr_2O_3 (> 0.1 wt%), with an average concentration of 0.40 wt% and ranging up to 1.12 wt% (Fig. 10). Chromium oxide is a strong colorant, and it only needs to be present in trace amounts in order to produce a yellow stain in the glaze (Henshaw 2010). The chromium is introduced into the glaze from reactions with chromite particles used as colorants and painted onto the underlying white slip. The yellow color occurs due to the digestion of chromite particles into the overlying lead glaze (Henshaw 2010). While no methods were used in this study that identified mineral phases, Holakooei et al. (2019) examined yellow-staining black ware by μ-Raman and identified the presence of chrome yellow ($PbCrO_4$) in the glazes (Holakooei et al. 2019, p. 768).

Two Early Islamic wares have been documented to use a chromium-based colorant: Yellow-staining black ware, known to be produced in Nishapur in the 10th c. CE (Watson, 2004), and Samanid slipwares with an olive/khaki-green slip (Henshaw, 2010). These two techniques can be seen on K142 and K175, in Fig. 11 and Fig. 12, respectively. Yellow-staining black ware is characterized as having clear pale lemon to full yellow color that is strongest in color near the black-painted decoration (Wilkinson 1975, p. 213). The painted decoration has a diffuse appearance (Fig. 11) and is applied as a thin paint composed of chromite particles that can separate into visible specks. The olive-slipped wares, on the other hand, have the chromium

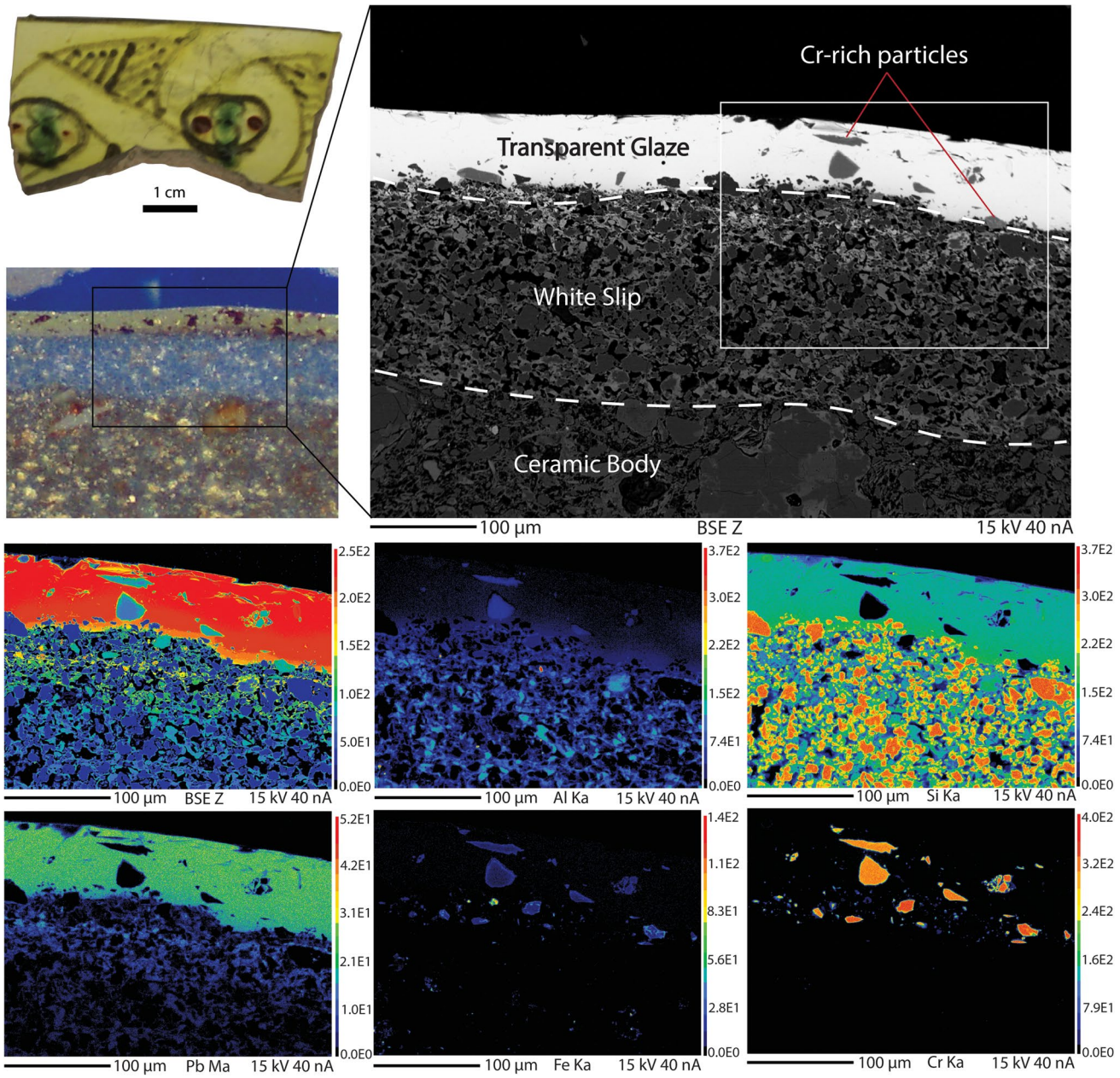

Fig. 11 Electron microprobe elemental mapping of the brown/black glaze on K142 showing the distribution of Al, Si, Pb, Fe, and Cr in the glaze and slip of the sample. Scale bar represents 100 µm. The white box on the BSE image indicates the mapped region, and white dashed lines indicate boundaries between the glaze, the white slip, and ceramic body

colorant applied as a thick slip rather than the thin paint. The slip is composed of chromite particles along with added clay and quartz. For K175, the olive-colored slip has a thickness of approximately 50 µm (Fig. 12), and Henshaw (2010) reported a thickness of around 100 µm in her analysis of olive-slipped ceramics from the Ferghana valley.

Measurement of the composition of the high chromium particles by EPMA indicates that they are a variety of magnesian aluminian chromite ($(Fe,Mg)(Cr,Al)_2O_4$), with an average composition of 20 wt% MgO, 5 wt% Fe_2O_3, 13 wt% Al_2O_3, and 60 wt% Cr_2O_3.

Seventeen samples have over 3 wt% Fe_2O_3 in the glaze. Iron is commonly found in lead glazes and generally needs to be in high concentrations (> 1 wt%) to impart color on the samples. The average composition was 5.01 wt% but ranged up to 10.26 wt%. Two of the samples (K009 and K181) had black and brown designs with significant concentrations of iron, manganese, and chromium, while eight of the samples (K048, K069, K070, K073, K076, K079, K182, and 186)

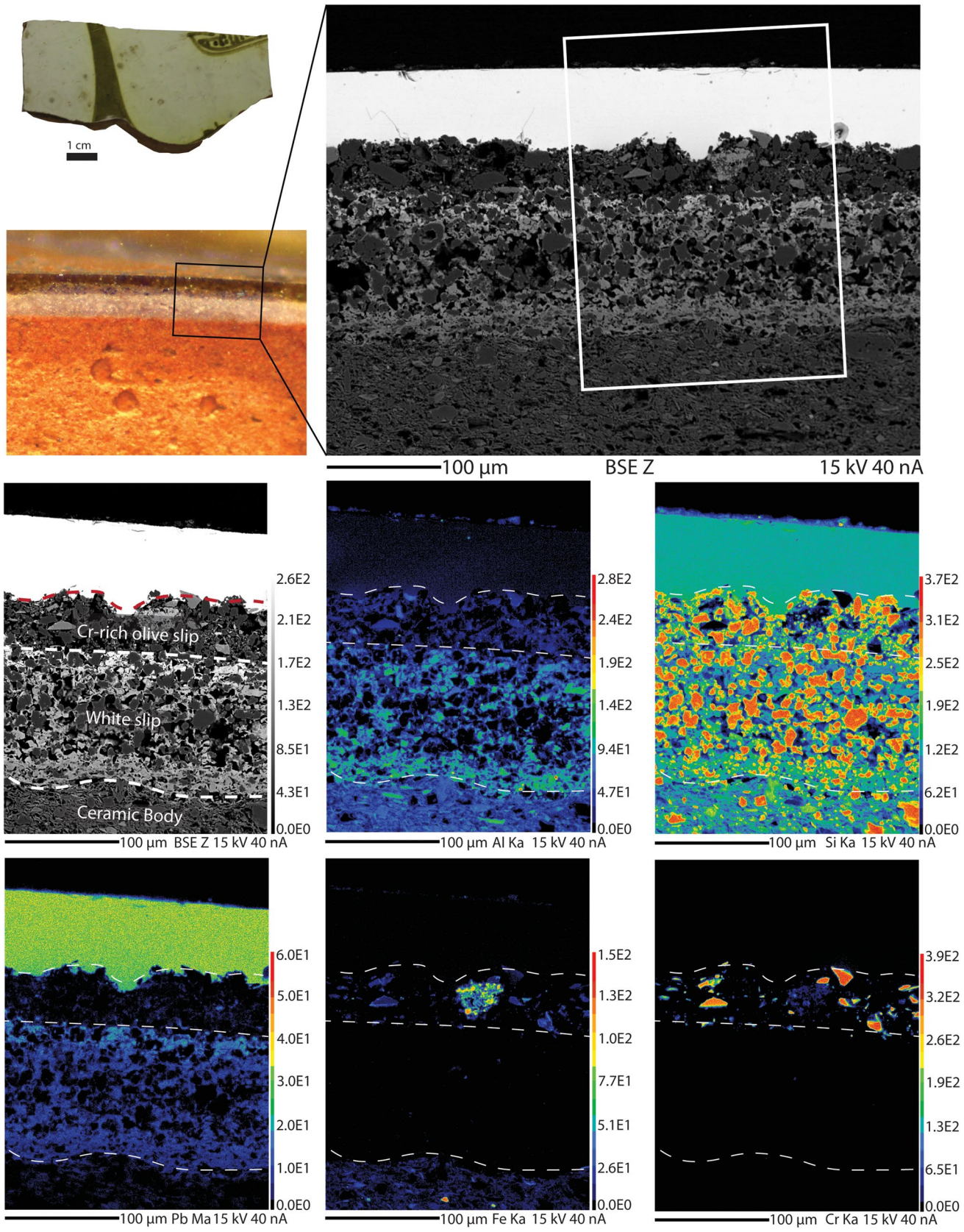
1 cm
100 µm BSE Z 15 kV 40 nA
Cr-rich olive slip
White slip
Ceramic Body
2.6E2
2.1E2
1.7E2
1.3E2
8.5E1
4.3E1
0.0E0
100 µm BSE Z 15 kV 40 nA
2.8E2
2.4E2
1.9E2
1.4E2
9.4E1
4.7E1
0.0E0
100 µm Al Ka 15 kV 40 nA
3.7E2
3.1E2
2.5E2
1.9E2
1.2E2
6.2E1
0.0E0
100 µm Si Ka 15 kV 40 nA
6.0E1
5.0E1
4.0E1
3.0E1
2.0E1
1.0E1
0.0E0
100 µm Pb Ma 15 kV 40 nA
1.5E2
1.3E2
1.0E2
7.7E1
5.1E1
2.6E1
0.0E0
100 µm Fe Ka 15 kV 40 nA
3.9E2
3.2E2
2.6E2
1.9E2
1.3E2
6.5E1
0.0E0
100 µm Cr Ka 15 kV 40 nA

◂**Fig. 12** Electron microprobe elemental mapping of the olive glaze on K175 showing the distribution of Al, Si, Pb, Fe, and Cr in the glaze and slip of the sample. Scale bar represents 100 µm. The white box on the BSE image indicates the mapped region, and white dashed lines indicate boundaries between the glaze, Cr-rich olive slip, white slip, and ceramic body

had both manganese and iron in the brown and black decoration. Three samples, K047, K050, and K067, have a light-yellow transparent glaze and have elevated concentrations of Sb_2O_5 (> 0.25 wt%).

High Bi samples

Twenty samples have Bi concentrations above 100 ppm (Table 4). The Bi concentration does not vary significantly by glaze color, although there is some variation observed in K129. Bi is a common component in lead ores and is one of the main trace elements found in archaeological lead and silver materials. While Bi is found in lead-rich archaeological artefacts, is it usually below 100 ppm and often below 20 ppm (L'Heritier et al. 2015).

Lead isotope analysis

The lead isotope ratios of glaze samples determined in this study are shown in the $^{208}Pb/^{204}Pb$ versus $^{206}Pb/^{204}Pb$, $^{207}Pb/^{204}Pb$ versus $^{206}Pb/^{204}Pb$, and $^{207}Pb/^{204}Pb$ versus $^{208}Pb/^{204}Pb$ plots seen in Fig. 13 and are reported in Table 5. The data reveal that most of the samples ($n = 23$) behave as a single group with values that range from 37.6409 to 38.2905, 15.5229 to 15.6088, and 17.4122 to 18.2383 for $^{208}Pb/^{204}Pb$, $^{207}Pb/^{204}Pb$, and $^{206}Pb/^{204}Pb$, respectively. A cluster of eight samples (K050, K066, K068, K088, K183, K195, K198, K199) have a similar isotopic signature that has a lower ratio $^{208}Pb/^{204}Pb$ and $^{206}Pb/^{204}Pb$ compared to the main group. This cluster's isotope values range from 37.0331 to 37.1862, 15.5280 to 15.5485, and 17.2009 to 17.3249 for $^{208}Pb/^{204}Pb$, $^{207}Pb/^{204}Pb$, and $^{206}Pb/^{204}Pb$, respectively. The sherds in this cluster all date to the earlier production period (9–12th c.). Five of these ceramics are from Aktobe. Two of the samples recovered from the ceramic production area at Aktobe (K198 and K199) fall within this cluster, but the third sample, K200, is more radiogenic and belongs to the main group. Two samples, K010 and K149, have very different isotopic signatures from the main group or the cluster and behave independently, with K010 having a high $^{208}Pb/^{204}Pb$ ratio (38.9206) and K149 having a low $^{207}Pb/^{204}Pb$ ratio (15.4561) (Fig. 13). There is no strong indication of shifts in the data based on the period of production, as can be seen in Fig. 13. The 14–15th c. ceramics (K027 and K028) from Aspara have very similar isotopic values but fall within the larger range of data for the 9–12th c. ceramics. There is also no differentiation in the data between the transparent and opaque wares, which both types of glaze present in the main group of samples and the cluster of eight. This suggests that there is not a distinction made between the lead used for transparent versus opaque glazed wares.

Identification of lead ore sources

To identify possible ore sources for the lead glazes, the isotopic data were compared to sources in the ore database compiled by Killick et al. (2020). Additional data for ore sources from Brill et al. (1997), Chegini et al. (2000), Ehya (2014), Merkel (2016), Nezafati (2006), and Pernicka et al. (2011) were included. This resulted in a comparative database of over 11,241 ore samples.

Given the attested long-distance transport of possible lead sources, samples were compared to ore deposits from the four closest tectonic zones to southern Kazakhstan to determine potential sources, including the Eastern European Craton ($n = 14$), the CAOB ($n = 1942$), the North China Craton ($n = 968$), and the Tethyan zone ($n = 856$) (Fig. 2). The samples had the strongest similarities to ore sources from the CAOB, although there were some sources that matched closest to the North China Craton (Fig. 14). The North China Craton and CAOB have significant overlap in isotopic signatures (Fig. 14). While it is not impossible that potters were importing lead from Northeastern China in this period, it has so far not been attested to. Given the isotopic similarity between the glazed samples and ore sources in the geographically closer CAOB tectonic zone, ore deposits from the North China Craton and Eastern European Craton were ruled out as likely sources.

Euclidean distances of the measured Pb isotope values ($^{208}Pb/^{204}Pb$, $^{207}Pb/^{204}Pb$, and $^{206}Pb/^{204}Pb$) were calculated to determine the nearest neighbors from the comparison database and identify likely sources using the Gauss 8.0 program. The routine identifies the nearest neighbors based on the following formula:

$$d^2 = (a_i - a_0)^2 + (b_i - b_0)^2 + (c_i - c_0)^2$$

where d is the straight distance between two specimens; a_i, b_i, c_i isotopic ratios $^{208}Pb/^{204}Pb$, $^{207}Pb/^{204}Pb$, and $^{206}Pb/^{204}Pb$ for sample i; and $a_0, b_0, c_0 \ldots z_0$ isotopic ratios $^{208}Pb/^{204}Pb$, $^{207}Pb/^{204}Pb$, and $^{206}Pb/^{204}Pb$ for sample 0. For each sample, the ten ore samples with the smallest values for d relative to other ore samples in the lead isotope database were identified and are listed in the Supplementary Information. Ore samples from the regions of the CAOB that are located most closely to the sites in southern Kazakhstan (Fig. 2) were initially compared, including deposits in the Balkhash metallogenic belt ($n = 38$), Bozshekol-Chengiz arc ($n = 3$), Chatkal-Kurama terrene ($n = 24$), Northern Tianshan ($n = 63$), Middle Tianshan ($n = 56$), and Southern Tianshan

Table 4 Description of samples with elevated concentrations of Bi (> 100 ppm)

ANID	Site	LIA	Glaze color	Bi (ppm)
K007	Lower Barskhan	x	Transparent	222.9
			Brown	312.4
			Green	304.1
K029	Aspara		Opaque blue	405.2
K079	Aktobe		Transparent	248.2
			Black	228.5
K099	Bektobe		Transparent	102.8
K125	Lower Barskhan		Transparent	774.0
			Light green	978.3
K126	Lower Barskhan		Transparent	142.3
K129	Lower Barskhan	x	Transparent	113.3
			Brown	440.1
			Yellow	281.9
K143	Tamdy		Light green	1066.3
K146	Tamdy		Green	246.0
K168	Merki	x	Light green	537.4
K178	Taraz		Opaque brown	630.2
			Opaque red	559.9
			Opaque white	515.9
K185	Taraz		Black	1011.7
			Green	962.1
K193	Akyrtas		Green	176.8
K194	Akyrtas		Transparent	107.9
K205	Sayram	x	Opaque green	147.5
K206	Bektobe		Brown	125.3
K210	Lower Barskhan		Light green	504.4
			Red	597.4
			Yellow	540.6
K211	Lower Barskhan		Light green	782.0
K212	Lower Barskhan	x	Opaque yellow	717.7
K213	Lower Barskhan		Opaque yellow	652.2

($n = 73$) districts (Table 6 and Fig. 15). The district termed Tianshan-Beishan ($n = 153$) reported by Hsu and Sabatini (2019) was also included in the statistical analysis independently from the Tianshan regions as it was not possible to determine each ore source in the database relation to the Northern, Middle, and Southern regions of Tianshan. Likely sources were identified through both direct comparison of Euclidean distances between the glaze and ore sources and visual comparison of glaze and ore sources isotopic signatures on $^{208}Pb/^{204}Pb$ vs. $^{206}Pb/^{204}Pb$, $^{207}Pb/^{204}Pb$ vs. $^{206}Pb/^{204}Pb$, and $^{207}Pb/^{204}Pb$ vs. $^{208}Pb/^{204}Pb$ three-isotope plots. The Euclidean nearest neighbors are reported in Table 7, and the specific deposits are indicated where appropriate.

Thirty-one of the thirty-three samples had a nearest neighbor from the selected deposits. The main group of samples had similar isotopic signatures to deposits across the different CAOB regions as they have overlapping signatures (Fig. 15). Some of the samples did match to specific deposits in the region (Table 7). K007 has a similar isotopic signature to the deposit of Shijinpo in the Beishan portion of the Tianshan-Beishan district. K048 and K152 both had a similar isotopic signature to the deposit of Kanling, which is located in the Southern Tianshan southwest of the city of Aksu (Fig. 16). K049, K128, and K168 all had similar isotopic ratios to ores from Awanda, which lies on the southern edge of the Tianshan mountains near the Kucha Oasis. K142 had a similar isotopic signature with Wulagan, which is in the Southern Tianshan and is located west of the city of Kashgar. K129 and K184 both have similar isotopic signatures to the deposit of Kendenggao'er in the Northern Tianshan (Fig. 16).

The cluster of eight samples (K050, K066, K068, K088, K183, K195, K198, K199) has a very discrete isotopic signature that matches only with that of the Caixiashan deposit in the Middle Tianshan district (Fig. 16). For the two outliers, K010 did have an isotopic signature similar to one deposit in the Southern Tianshan district a (Sawayaerdun) and one deposit in the Beishan district (Jinwozi), although neither are similar enough to assign as a likely ore source. There were no deposits in the selected districts of the CAOB whose Euclidean distance was near K149.

The glaze samples were also tested against ore deposits that have archaeological evidence of mining and metallurgy during the 7–12th c. CE. Three ore deposits, Lashkerek in Uzbekistan (Merkel 2016), Aktyuz in Kyrgyzstan (Chiaradia et al. 2006), and Pamir in Tajikistan (Pavlova and Borisenko 2009), were known silver mines in the Medieval Period and have published isotopic data (Fig. 16 and Fig. 17). Additionally, lead slag from the site of Tunket in Uzbekistan, which was a medieval city with extensive evidence of silver production, was included (Merkel 2016). The main group of samples display a strong similarity to the isotopic signature of lead ores at known silver mines in the Tianshan mountains (Fig. 17). Seventeen samples had an isotopic signature similar to the lead ores and slags recovered from the Lashkerek and Tunket in Uzbekistan (Fig. 17). Four samples (K087, K152, K156, K200) had similar isotopic signatures to the ore deposit of Aktyuz in the Northern Tianshan district (Fig. 17). The cluster of eight samples did not have a similar signature to any of the known Medieval mines, and none of the glaze samples had a similar isotopic signature to the lead ores in the Pamir region (Fig. 17).

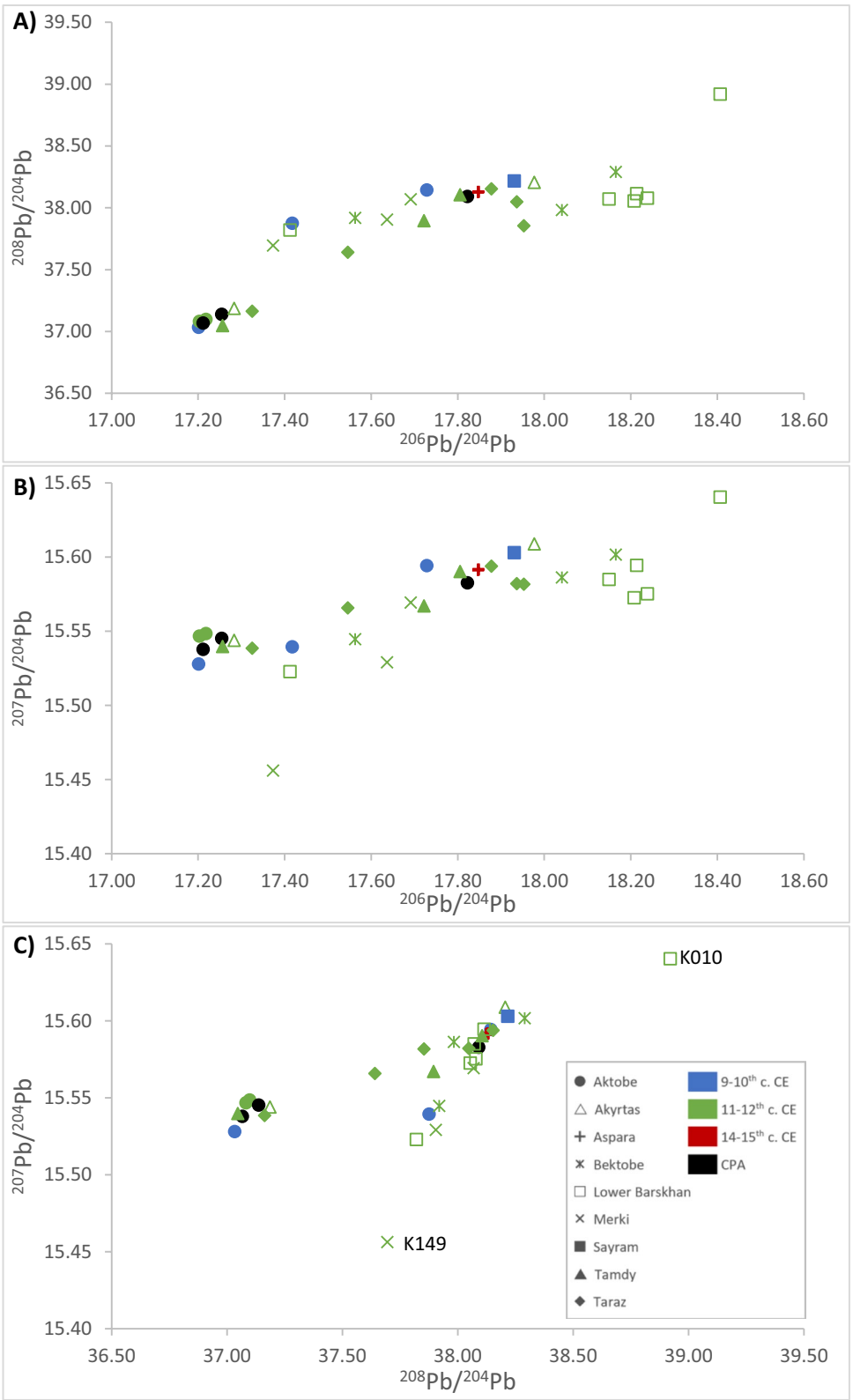

Fig. 13 **A** $^{208}Pb/^{204}Pb$ vs. $^{206}Pb/^{204}Pb$, **B** $^{207}Pb/^{204}Pb$ vs. $^{206}Pb/^{204}Pb$, **C** $^{207}Pb/^{204}Pb$ vs. $^{208}Pb/^{204}Pb$ three-isotope plots for the lead glazes distributed by their find sites (symbols) and period of production (color of symbols). Blue indicates 9–10th c. ceramics, green 11–12th c. ceramics, red 14–15th c. ceramics, and black indicates it comes from a CPA (ceramic production area). 2σ errors less than the size of the symbols

Table 5 Lead isotopic values for the lead glazes on thirty-three ceramics from southern Kazakhstan. 2σ, 2 standard deviations (internal error). *L. Barskhan* Lower Barskhan

ANID	Site	Date (c. CE)	$^{208}Pb/^{204}Pb$	2σ	$^{207}Pb/^{204}Pb$	2σ	$^{206}Pb/^{204}Pb$	2σ
K007	L. Barskhan	11–12th	38.1144	0.0021	15.5946	0.0007	18.2132	0.0007
K009	L. Barskhan	11–12th	38.0543	0.0024	15.5726	0.0014	18.2078	0.0009
K010	L. Barskhan	11–12th	38.9206	0.0020	15.6404	0.0007	18.4066	0.0009
K027	Aspara	14–15th	38.1261	0.0024	15.5913	0.0008	17.8468	0.0009
K028	Aspara	14–15th	38.1310	0.0017	15.5918	0.0007	17.8477	0.0007
K048	Aktobe	9–10th	38.1435	0.0016	15.5943	0.0006	17.7282	0.0006
K049	Aktobe	9–10th	37.8755	0.0020	15.5395	0.0007	17.4173	0.0007
K049[a]	Aktobe	9–10th	37.8815	0.0022	15.5406	0.0007	17.4187	0.0007
K050	Aktobe	9–10th	37.0331	0.0021	15.5280	0.0007	17.2009	0.0008
K066	Aktobe	11–12th	37.0819	0.0018	15.5467	0.0007	17.2029	0.0007
K068	Aktobe	11–12th	37.0981	0.0017	15.5485	0.0006	17.2179	0.0007
K087	Tamdy	11–12th	37.8947	0.0020	15.5671	0.0007	17.7222	0.0007
K088	Tamdy	11–12th	37.0475	0.0015	15.5397	0.0006	17.2563	0.0007
K128	L. Barskhan	11–12th	37.8205	0.0016	15.5229	0.0006	17.4122	0.0007
K129	L. Barskhan	11–12th	38.0781	0.0021	15.5753	0.0008	18.2383	0.0008
K142	Tamdy	11–12th	38.1060	0.0030	15.5903	0.0010	17.8054	0.0010
K149	Bektobe	11–12th	37.6953	0.0020	15.4561	0.0007	17.3733	0.0007
K152	Bektobe	11–12th	38.0686	0.0029	15.5693	0.0011	17.6911	0.0013
K152[a]	Bektobe	11–12th	38.0687	0.0025	15.5694	0.0009	17.6914	0.0010
K156	Bektobe	11–12th	37.9055	0.0017	15.5292	0.0008	17.6368	0.0008
K168	Merki	11–12th	38.2905	0.0021	15.6017	0.0008	18.1652	0.0009
K169	Merki	11–12th	37.9191	0.0023	15.5447	0.0008	17.5628	0.0009
K171	Merki	11–12th	37.9830	0.0018	15.5862	0.0006	18.0409	0.0010
K175	Taraz	10–12th	37.8542	0.0019	15.5818	0.0007	17.9527	0.0007
K177	Taraz	10–12th	37.6409	0.0025	15.5658	0.0010	17.5460	0.0010
K179	Taraz	10–12th	38.1537	0.0024	15.5938	0.0010	17.8779	0.0011
K183	Taraz	10–12th	37.1631	0.0021	15.5385	0.0008	17.3249	0.0008
K184	Taraz	10–12th	38.0479	0.0025	15.5821	0.0009	17.9363	0.0009
K192	Akyrtas	11–12th	38.2061	0.0025	15.6088	0.0008	17.9771	0.0009
K192[a]	Akyrtas	11–12th	38.2067	0.0026	15.6096	0.0009	17.9779	0.0011
K192[b]	Akyrtas	11–12th	38.2044	0.0019	15.6096	0.0007	17.9758	0.0007
K192[a,b]	Akyrtas	11–12th	38.2122	0.0018	15.6111	0.0007	17.9788	0.0008
K195	Akyrtas	11–12th	37.1862	0.0025	15.5439	0.0009	17.2829	0.0010
K198	Aktobe–Kiln	10–12th	37.1379	0.0027	15.5452	0.0009	17.2547	0.0009
K199	Aktobe–Kiln	10–12th	37.0671	0.0027	15.5379	0.0010	17.2115	0.0011
K200	Aktobe–Kiln	10–12th	38.0907	0.0018	15.5828	0.0006	17.8223	0.0006
K205	Sayram	9th	38.2171	0.0024	15.6031	0.0008	17.9307	0.0010
K212	L. Barskhan	11–12th	38.0709	0.0016	15.5850	0.0006	18.1495	0.0006

[a]Replicate sample.

[b]Sample analyzed both in dry and wet plasma.

Discussion

Glaze composition and technology

Transparent high-lead glazes

The transparent high-lead glaze recipe is very similar to lead glazes from other Central Asian sites in the Early Islamic Period, including the sites of Termez and Akhisket in modern-day Uzbekistan (Henshaw 2010; Molera et al. 2020). The transparent lead glazes from these sites, however, behave as a single group, and no chemical differentiation is observed between glazes of different periods of production, provenance, or ware when colorants are removed. If potters were using strictly local raw materials to produce the high-lead glazes, we would expect to see differentiation in

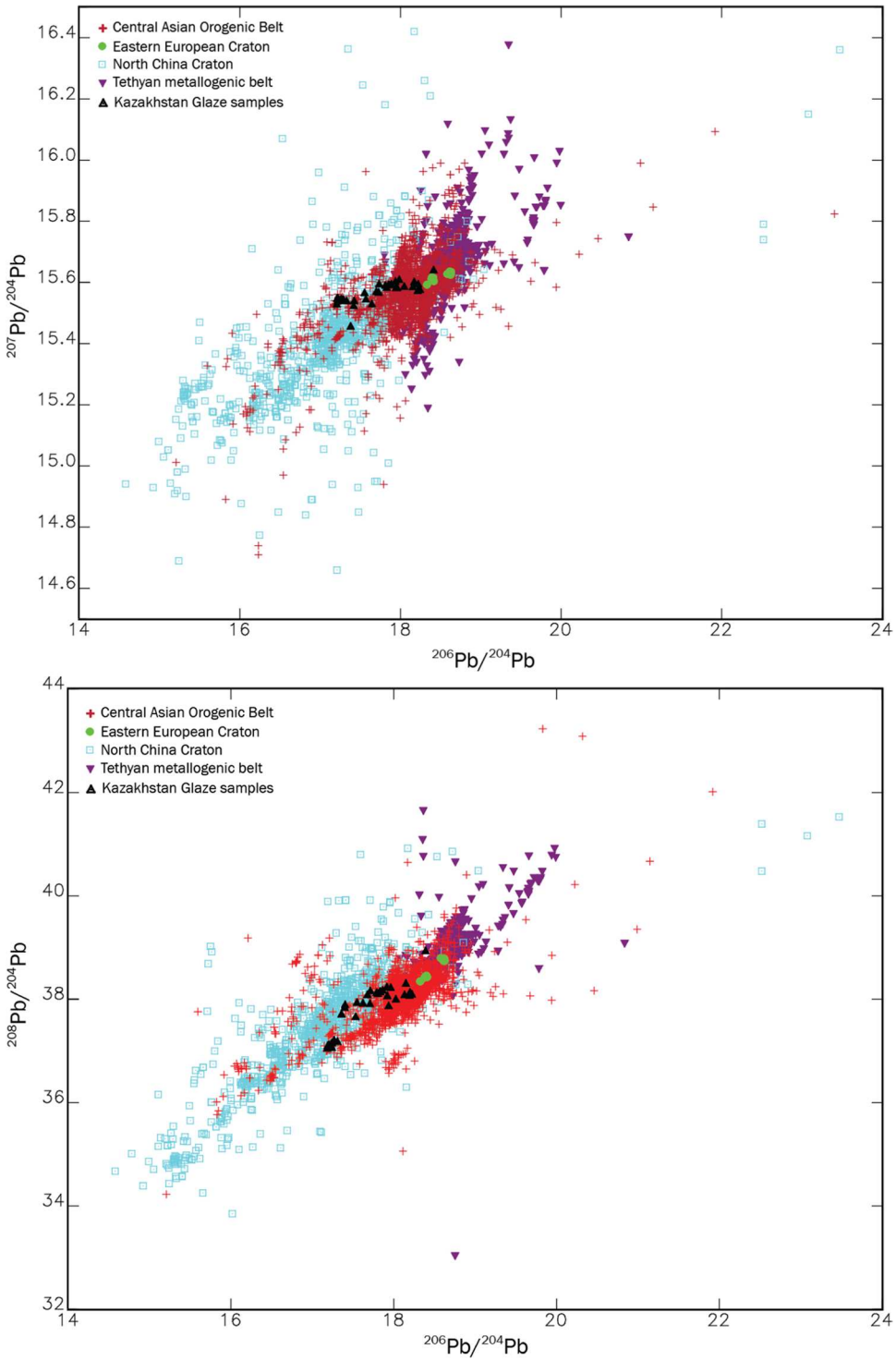

Fig. 14 (*above*) $^{207}Pb/^{204}Pb$ vs. $^{206}Pb/^{204}Pb$ and (*below*) $^{208}Pb/^{204}Pb$ vs. $^{206}Pb/^{204}Pb$ three-isotope plots for the Kazakhstan lead glaze samples in relation to lead isotope data from the CAOB, Eastern European Craton, North China Craton, and Tethyan metallogenic belt. Data extends beyond the area of the plot

the trace elements of the glazes based on different geologies near the centers of production. The elements with the greatest differentiation in the transparent glazes, as determined by the PCA, are Bi, Sb, Ag, Sn, In, As, Cl, Mo, and Zn (see Supplementary Information). These elements are commonly associated with lead ores (Walton 2004), and the amount of Bi, Sb, Ag, As, Cl, Sn, and Zn in a lead glaze is predominantly due to (1) the original lead ore that is used and (2) how it is processed prior to being mixed with the other glaze raw materials and applied to the ceramic body. From these results, it is apparent that the lead sources for the glazes are those responsible for the greatest degree of differentiation between the samples, and not the other primary components of the lead glaze (i.e., the silica source).

Table 6 Deposits in the southwestern portion of the CAOB used in comparative analyses

District	Location	Deposit	*n*	References
Balkhash metallogenic belt	Kazakhstan	Aktogay	8	Syromyatnikov et al. (1988)
		Aydarly	7	Syromyatnikov et al. (1988)
		Borly	8	Syromyatnikov et al. (1988)
		Koksay	4	Syromyatnikov et al. (1988)
		Kounrad	11	Syromyatnikov et al. (1988) and Cao et al. (2018)
Bozshekol-Chengiz arc	Kazakhstan	Boshchekul	3	Syromyatnikov et al. (1988)
Chatkal-Kurama	Uzbekistan	Agata	4	Chernyshev et al. (2017)
		Chauli	20	Chernyshev et al. (2017)
Middle Tianshan	Uzbekistan	Kalmakyr	2	Chiaradia et al. (2006)
	Uzbekistan	Kochbulak	1	Chiaradia et al. (2006)
	Kyrgyzstan	Kumtor	1	Chiaradia et al. (2006)
	Kyrgyzstan	Makmal	3	Chiaradia et al. (2006)
	Uzbekistan	Uchkulach	2	Chiaradia et al. (2006)
	Uzbekistan	Ustarasay	1	Chiaradia et al. (2006)
	Xinjiang	Caixiashan	19	Li et al. (2018)
	Xinjiang	Hongyuan	11	Lu et al. (2018)
	Xinjiang	Saridala	16	Zhang et al. (2018)
Northern Tianshan	Xinjiang	Kangguertage	2	Hong et al. (2003)
	Kyrgyzstan	Aktyuz	2	Chiaradia et al. (2006)
	Xinjiang	Axi	2	Chiaradia et al. (2006)
	Kyrgyzstan	Boordu	4	Chiaradia et al. (2006)
	Kyrgyzstan	Chonur	2	Jenchuraeva (1997)
	Kyrgyzstan	Taldybulak	3	Chiaradia et al. (2006)
	Xinjiang	Kendenggao'er	39	Wang et al. (2018)
	Xinjiang	Qunjsai	9	Zhao et al. (2018)
Southern Tianshan	Uzbekistan	Amantaitau	4	Chiaradia et al. (2006)
	Xinjiang	Awanda	29	Ding et al. (2014)
	Uzbekistan	Daugyztau	4	Chiaradia et al. (2006)
	Uzbekistan	Guzhumsay	5	Chiaradia et al. (2006)
	Uzbekistan	Mardjanbulak	1	Chiaradia et al. (2006)
	Uzbekistan	Muruntau	2	Chiaradia et al. (2006)
	Uzbekistan	Sarmich	6	Chiaradia et al. (2006)
	Uzbekistan	Sarytau	1	Chiaradia et al. (2006)
	Xinjiang	Sawayaerdun	20	Chen et al. (2012) and Hong et al. (2003)
	Uzbekistan	Zarmitan	1	Chiaradia et al. (2006)
Tianshan-Beishan	Xinjiang	Abei	7	Hsu and Sabatini (2019)
	Xinjiang	Bogutu	7	Hsu and Sabatini (2019)
	Gansu	Huaniushan	27	Hsu and Sabatini (2019)
	Xinjiang	Huoshenbulake	7	Hsu and Sabatini (2019)
	Xinjiang	Kalagailei	1	Hsu and Sabatini (2019)
	Xinjiang	Kangguer	2	Hsu and Sabatini (2019)
	Xinjiang	Kanling	14	Hsu and Sabatini (2019)
	Xinjiang	Kuergasheng	6	Hsu and Sabatini (2019)
	Xinjiang	Lamasu	1	Hsu and Sabatini (2019)
	Xinjiang	Qiongbulake	3	Hsu and Sabatini (2019)
	Xinjiang	Qixing	4	Hsu and Sabatini (2019)
	Xinjiang	Shalitashen	6	Hsu and Sabatini (2019)
	Gansu	Shijinpo	1	Hsu and Sabatini (2019)
	Gansu	Shijinpochuang	1	Hsu and Sabatini (2019)
	Xinjiang	Tabei	3	Hsu and Sabatini (2019)
	Xinjiang	Wulagen	49	Hsu and Sabatini (2019)
	Xinjiang	Xiaoxigong	3	Hsu and Sabatini (2019)
	Xinjiang	Jinwozi	11	Zhang et al. (2014)

From technological studies of these ceramics (Klesner et al. 2021), as well as other research on Islamic glazed ceramics from Central Asia, we know that lead glaze was made by pre-fritting lead oxide and silica, and not by the direct application of lead oxide onto the slip (Walton and Tite 2010; Tite et al. 2015; Molera et al. 2020; Ting and Taxel 2020). Abu'l-Qusim Kashani's treatise on pottery production from 1301 CE describes the lead glaze as being

applied as a glaze frit which has been ground, finely sifted, and mixed with water (Allan 1973). The fritting of PbO and SiO_2 was also noted by Henshaw (2010) for the ceramics from Akhsiket. It is not known, however, if Islamic potters are starting with lead or lead-containing compounds and if they are roasting the lead prior to fritting with SiO_2. Henshaw (2010) described the most probable source of lead for glaze production as galena, which was roasted prior to the fritting with silica, and however also mentioned that litharge, which was produced as a byproduct of silver cupellation, could have been used in the production of the glaze.

Opaque glazes

The most unexpected observation in the technological analysis is the variation in opacifying agents in the opaque glazed sherds. Only two of the samples have a tin-opacified glaze, compared to the four samples with an antimony-opacified glaze and four with an antimony- and tin-opacified glaze. The first opaque lead glazes in the Islamic world, produced in Egypt between the 7th and early 9th c. CE, were made with tin particles as the opacifying agent (Watson 2014; Tite et al. 2015; Matin et al. 2018; Ting and Taxel 2020). The tin-opacified glazes could be either yellow (opacified by lead stannate, $Pb(Sn,Si)O_3$) or white (opacified by SnO_2 crystals), depending on the composition and firing temperature of the glaze. The yellow opaque glazes were the first to be produced, followed by the white opaque glazes, and both technologies spread throughout the Islamic world in the 9th and 10th c. CE. White tin-opacified glazes became the mainstream glazing technology used in the Islamic world during the Medieval Period (Matin 2019). The fact that only 2 of the 10 opaque glazes in this sample are tin-opacified is thus unexpected.

The use of antimony in an opaque glaze, as seen in samples K106, K213, K196, and K178, is unusual for the Early Islamic Period in the eastern Islamic world. In the second half of the 9th c. CE, workshops in Fustat (Egypt) began using yellow lead antimonate as a glaze opacifier, rediscovering the technology used to opacify glass and alkaline glazes in the Roman period (Salinas et al. 2019). The opaque yellow glaze and opaque amber and green glazes on the multi-colored glazed finewares were opacified with lead antimonate particles (Salinas et al. 2019). The reintroduction of lead antimonate as an opacifier is attributed to local innovation of the Egyptian potters experimenting with stibnite (Sb_2S_3) and galena (PbS) minerals to produce new glaze colors and is potentially linked to the potters using an antimony-containing source of lead in the production of their glazes (Salinas et al. 2019). This technology appears to have spread in the Western edges of the Islamic world to Tunisia, the Mediterranean basin (Salinas et al. 2019), and Yemen (Hallett et al. 1988), but not into the eastern Islamic world. Henshaw (2010) notes that antimony yellow was not widely used in Central Asia, and not found in the Ferghana valley at all (Henshaw 2010, p. 258). Holakooei et al. (2019) also note that while two treatises on the production of glazes, Nayshaburi (12th c. CE) and Abu'l Qasim Kashani (1301 CE), mention a substance named *ithmid* or *athmad* (traditionally translated as antimony sulfide) that was used to produce a yellow glaze, no antimony yellow glaze has been recorded in Iran (Allan et al. 1973; Holakooei et al. 2019). The antimony-opacified glazes from northern Central Asia are not likely linked to the reintroduction of antimony glazed ceramics in Egypt but likely represent a similar, independent discovery of antimony opacifiers by Central Asia potters.

The occurrence of both tin- and antimony-opacified ceramics is also unattested in this region in the Early Islamic Period. The use of both tin and antimony opacifiers has been noted on glazed ceramics but utilizing a different glaze technology. In the Egyptian polychrome glazed ceramics from the 9–11th c. CE., colored glazes opacified with antimony were applied over white opaque glaze opacified with SnO_2 (Salinas et al. 2019). The glaze colors that have antimony do not normally have tin present (Salinas et al. 2019, p. 7). Tin can be seen incorporated into the lead antimonate particles but only in particles close to the underlying white glaze layer, and it is evident that the antimony and tin are two distinct opacifiers and chosen by the potters for different decorative components of the glaze. The tin- and antimony-opacified glazes in this study, however, show even distribution of the antimony and tin oxide particles throughout the glaze depth (Fig. 8 and Fig. 9). The consistent ratios of Sb_2O_5 to SnO_2 in multiple glaze colors on single sherds indicate that the opacifier is independent of the colorants used in the glaze recipes. The co-occurrence of the two opacifying agents thus does not appear to be from application of multiple glaze layers with distinct opacifying agents; instead, the potters are adding them together as a single opacifying agent.

The choice of antimony and antimony-tin based opacifiers could be due to availability of the raw material in the region. In Central Asia, the main silver ore sources all contain the unusual Ag-Sb mineralization type (Pavlova and Borisenko 2009), which contain high-Sb sulfosalts, Sb sulfides, and native antimony. Two of these sources, the Talas silver ore district and the Pamir silver ore district were known silver producers in antiquity (Pavlova and Borisenko 2009). If local craftsmen were sourcing their silver or lead ore from these mining regions, it is possible that they were also obtaining antimony to use as a glass and glaze opacifier.

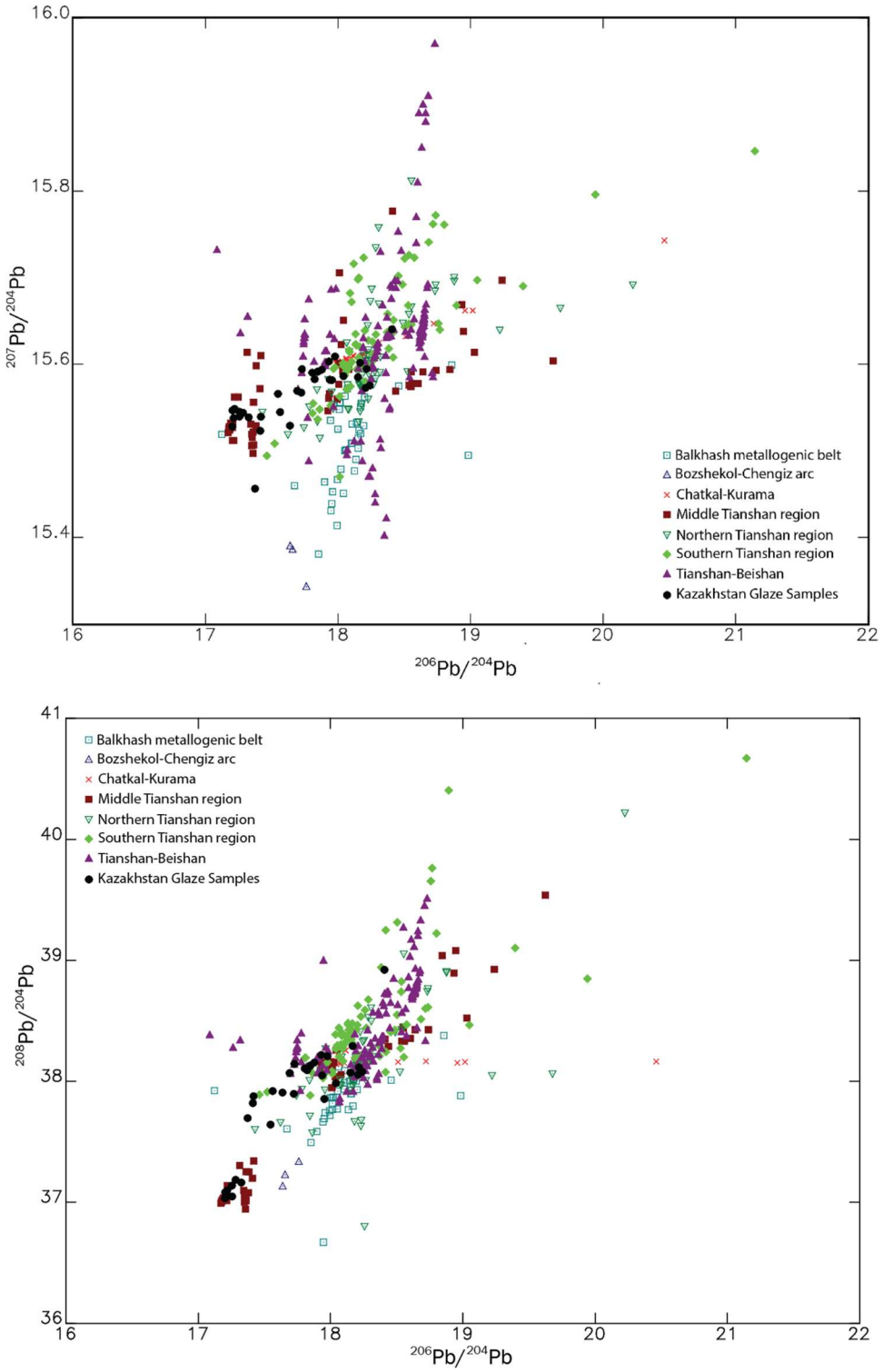

Fig. 15 (*above*) $^{207}Pb/^{204}Pb$ vs. $^{206}Pb/^{204}Pb$ and (*below*) $^{208}Pb/^{204}Pb$ vs. $^{206}Pb/^{204}Pb$ three-isotope plots for the Kazakhstan lead glaze samples in relation to districts in the southwestern section of the CAOB

Colorants

The choice of colorants employed in the opaque and transparent lead glazes does vary based on period of production and provenance and likely reflects local sourcing of different colorants. For the locally produced ceramics in southern Kazakhstan, only copper, iron, and manganese were observed as colorants. These are common colorants used in the production of polychrome lead glazes and were used on Early Islamic lead-glazed ceramics from across the Islamic world (Gradmann et al. 2015). Two colorants, cobalt and chromium, were only observed on

Table 7 Nearest Euclidean neighbors for the districts of the CAOB in the vicinity of the Chu river valley. Specific deposits in the districts are indicated where appropriate.[1]

ANID	Site	Date (c. CE)	Euclidean nearest neighbors
K007	Lower Barskhan	11–12th	Tianshan-Beishan (Shijinpo), Northern Tianshan, Chatkal-Kurama
K009	Lower Barskhan	11–12th	Northern Tianshan, Balkhash metallogenic belt, Tianshan-Beishan
K010	Lower Barskhan	11–12th	Southern Tianshan, Tianshan-Beishan
K027	Aspara	14–15th	Tianshan-Beishan, Southern Tianshan, Northern Tianshan
K028	Aspara	14–15th	Tianshan-Beishan, Southern Tianshan, Northern Tianshan
K048	Aktobe	9–10th	Tianshan-Beishan (Kanling)
K049	Aktobe	9–10th	Southern Tianshan (Awanda)
K050	Aktobe	9–10th	Middle Tianshan (Caixiashan)
K066	Aktobe	11–12th	Middle Tianshan (Caixiashan)
K068	Aktobe	11–12th	Middle Tianshan (Caixiashan)
K087	Tamdy	11–12th	Northern Tianshan, Tianshan-Beishan
K088	Tamdy	11–12th	Middle Tianshan (Caixiashan)
K128	Lower Barskhan	11–12th	Southern Tianshan (Awanda)
K129	Lower Barskhan	11–12th	Northern Tianshan (Kendenggao'er), Tianshan-Beishan
K142	Tamdy	11–12th	Tianshan-Beishan (Wulagen), Southern Tianshan, Northern Tianshan
K149	Bektobe	11–12th	None
K152	Bektobe	11–12th	Tianshan-Beishan (Kanling), Northern Tianshan
K156	Bektobe	11–12th	None
K168	Merki	11–12th	Southern Tianshan (Awanda), Balkhash metallogenic belt, Tianshan-Beishan, Chatkal-Kurama
K169	Merki	11–12th	Southern Tianshan, Northern Tianshan
K171	Merki	11–12th	Middle Tianshan, Balkhash metallogenic belt, Southern Tianshan
K175	Taraz	10–12th	Northern Tianshan, Balkhash metallogenic belt, Southern Tianshan
K177	Taraz	10–12th	Northern Tianshan, Southern Tianshan
K179	Taraz	10–12th	Tianshan-Beishan, Northern Tianshan
K183	Taraz	10–12th	Middle Tianshan
K184	Taraz	10–12th	Northern Tianshan (Kendenggao'er), Southern Tianshan, Middle Tianshan, Tianshan-Beishan
K192	Akyrtas	11–12th	Southern Tianshan, Chatkal-Kurama, Middle Tianshan
K195	Akyrtas	11–12th	Middle Tianshan
K198	Aktobe–Kiln	10–12th	Middle Tianshan
K199	Aktobe–Kiln	10–12th	Middle Tianshan (Caixiashan)
K200	Aktobe–Kiln	10–12th	Tianshan-Beishan, Northern Tianshan, Southern Tianshan
K205	Sayram	9th	Tianshan-Beishan, Middle Tianshan, Southern Tianshan
K212	Lower Barskhan	11–12th	Northern Tianshan, Tianshan-Beishan, Balkhash metallogenic belt

[1]Deposits are indicated when either (1) all three lead isotope ratios for the sample and the ore sample are within the limit of the analytical error of ±0.1% for each lead isotope ratio or (2) all the Euclidean nearest neighbors are from the same ore deposit.

non-local ceramics. Cobalt was noted on one lead-glazed ceramic, and that dates to the later 14–15th c. Chromium was observed on two wares that were imported into the region: yellow-staining black ware ceramics and olive-slipped ceramics. High amounts of CuO (2.81 wt%) are present in the chromite particles on one sample, K009, from Lower Barskhan. Cu is not an element commonly associated with chromites, which have a general formula of $(Fe,Mg)(Cr,Al,Fe)_2O_4$. High levels of copper were also noted by Henshaw (2010) in an olive-slipped sample from Akhsiket, which had chromite particles with 1.2 wt% CuO. Holakooei et al. (2019) also identified elevated levels of copper in the chromite painted areas of glazed sherds from Afrasiyab (Samarkand), but saw no increase in copper levels in the chromite regions of sherds from Nishapur. The elevated concentrations of copper in the chromite-colored glazes maybe reflective of CuO being added to the glaze to create a greenish hue. This was investigated by Pernicka and Malissa (1980) who identified chromite colorants in the 12–14th c. CE alkali-glazed pottery from Nimruz, in the southwestern region of Afghanistan. Some of the chromite colorants in these ceramics also had substantial

Fig. 16 Location of the archaeological sites in southern Kazakhstan (red circle), major Silk Road trading centers in the period (green circle), and specific ore deposits mentioned in the text (blue circle)

concentrations of Cu, as well as elevated concentrations of Co. The authors attributed the elevated Cu concentration in the chromite particles as forming from a reaction in the firing process where CuO particles added to the glaze dissolved into the glass matrix and favorably concentrate in chromite particles (Pernicka and Malissa 1980). The phenomenon was further investigated by Tite (1989), who observed elevated concentrations of copper (3–22% CuO) and cobalt (0.5–16 wt% CoO) in chromites present in later the 15th c. Iznik pottery. He observed a clear inverse correlation between the depletion of Mn and Fe oxide contents of chromite particles with the elevated levels of Cu and Co oxides. This, along with the work of Pernicka and Malissa (1980), suggests that the Cu and Co that are present in the chromite particles in the glazes have been absorbed during the firing process and replaced the Mn and Fe in the chromite lattice (Tite 1989, p. 126).

These results suggest that K009 likely had some CuO added to the glaze, which was also observed on the chromite-colored ceramics from Afrasiyab and the Ferghana valley. This common technique could suggest that this sherd was produced in Transoxiana. Yellow-staining black ware sherds with a chromium colorant were also identified in this study, and this ware is known to be produced in Nishapur (Watson 2004), suggesting that they were importing specialty wares from the Greater Khorasan region.

Lead ore sources

The identification of specific lead ore sources for these glazes is difficult due (1) to the overlapping nature of the lead isotope ratios from different deposits in the region, (2) the complete absence of data on some ore deposits, and (3) the non-even distribution of comparative sources from across the different modern political regions. These are well attested difficulties with LIA (Killick et al. 2020; Medeghini et al. 2020). However, the results do allow for some identification of potential ore sources that were exploited for glaze production, as well as indicating avenues of future research.

Main group

As can be seen in Fig. 15, the ore deposits in the districts of the southern extent of the CAOB have overlapping isotopic signatures which make it difficult to isolate specific ore sources for the lead glaze. However, within the main group of samples, eight sherds had isotopic signatures that were very similar to five distinct deposits: Shijinpo (Hsu and Sabatini 2019), Kanling (Hsu and Sabatini 2019), Awanda (Ding et al. 2014), Wulagan (Hsu and Sabatini 2019), and Kendenggao'er (Wang et al. 2018) (Table 7). These deposits all are located within the modern political borders of Xinjiang and, except for Kendenggao'er, lie near the Silk Road passage that ran along the southern edge of the Tianshan mountains (Fig. 16). This route, which connects to the northern route at Tashkent in the west and Turfan and Urumqi in the east, ran through the oasis cities of Kucha, Aksu, and Kashgar. There is material evidence of cultural connections between the people living in southern Kazakhstan with Xinjiang beginning at least in the 8th c. CE. Graffiti from the palace at the site of Kulan (Fig. 16) depicts men wearing headdresses known from the 9–10th c. Turkic Uighurs who were settled in the northeastern region of Xinjiang (Akylbek et al. 2017). Other figures are depicted in similar headdresses to those known in both the northern and southern oases in Xinjiang from the 8th c. CE, including the Kucha

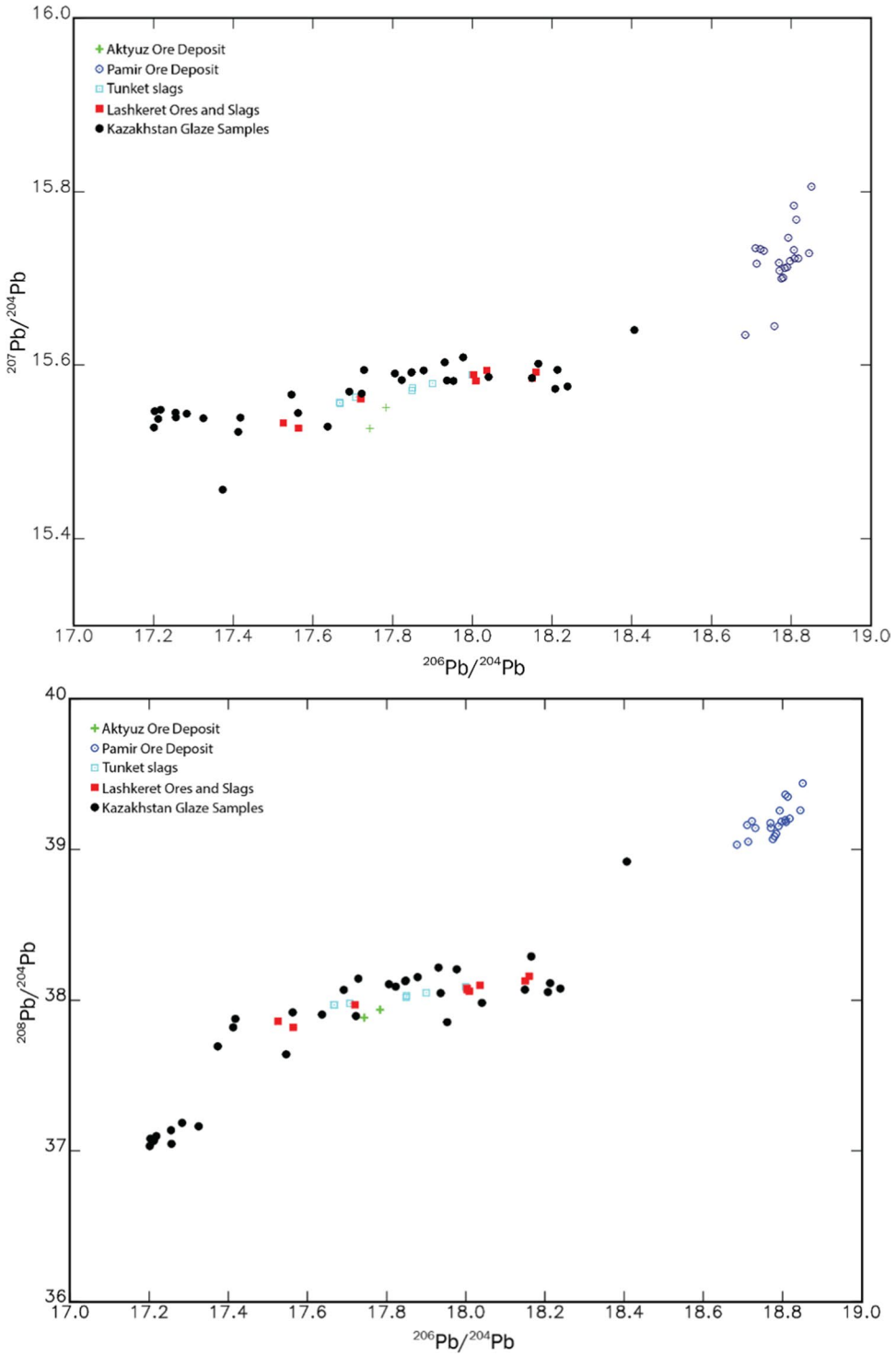

Fig. 17 (*above*) $^{207}Pb/^{204}Pb$ vs. $^{206}Pb/^{204}Pb$ and (*below*) $^{208}Pb/^{204}Pb$ vs. $^{206}Pb/^{204}Pb$ three-isotope plots for the Kazakhstan lead glaze samples in relation to contemporary mining sources in the region

oasis (Akylbek et al. 2017). Mining is attested in the region of Kucha from the 7th c. CE. Xuanzang, a Buddhist monk who traveled a portion of the silk road, documented the use of gold or silver coins in Kucha, as well as the mining of gold, copper, iron lead, and tin (Barisitz 2017, p. 57). The strongest connection of southern Kazakhstan to the Tarim Basin occurred beginning in the mid-10th c. CE, when the Karakhanid Khaganate rose to power and gained control of the western portion of the Tarim Basin including the cities of Aksu and Kashgar (Barisitz 2017, p. 87). The Karakhanids had their political center in the Semirechye region in southern Kazakhstan, and thus, if there were active mines in the western portion of the Tarim Basin, they could have been a possible source of lead for glazes produced in Semirechye.

The strong association with ore deposits in Xinjiang could also be an artifact of the relative number of ore sources with isotopic data published from Central Asia. Given modern political history, the regions that fall in the former Soviet Republics have been relatively understudied and under-published. In the comparative databases, there are ore sources documented from Kazakhstan ($n=91$), Kyrgyzstan ($n=15$), Uzbekistan ($n=64$), and Tajikistan ($n=22$). There is no lead isotope data from Turkmenistan and Afghanistan. From Xinjiang there are 529 comparative ore sources, greatly outnumbering the sources from other Central Asian regions.

The isotopic similarity of the main group of samples to known Medieval silver mines in the Tianshan mountains offer a more likely source for the lead ores used in the glaze production (Fig. 17). In the Early Islamic Period in Central Asia, silver coinage was widely minted and known, at least initially, for its high purity (Barisitz 2017). While silver coinage had been produced in Central Asia dating at least back to the Sassanians (Merkel 2016), it was the Samanids (9–10th c. CE) that dramatically increased the circulation of silver coins (Barisitz 2017, p. 78). The Samanids, whose territory included Transoxiana, Ferghana, Greater Khorasan, Afghanistan, and Khwarazm, had extensive mining activity throughout their territory. These included the mines in the Ferghana Basin that extracted iron, tin, silver, mercury, copper, and lead, among others; the mines the Pamir region that produced rubies, lapis lazuli, and silver; the mines of Tokharistan, which produced lead and sulfur; and the mines of Ilaq Shash, which were rich in gold and silver (Barisitz 2017, p. 80).

The Ilaq Shash region, in modern-day Tajikistan and Uzbekistan, was excavated beginning in the early 20th c., and there is extensive evidence for silver extraction, including crushed ores, slag heap, litharge (PbO), smelting furnaces, and cupels along with the tool miners would have used in these processes (Eniosova and Mitoyan 2011). The mine at Lashkerek was one of the largest and was reported to have 9,000 tons of slag, which Merkel (2016) characterized by LIA in his study of Samanid silver coins in Viking trading centers. The ore deposit is classified as polymetallic with native silver occurring in masses of up to 1 cm in diameter and in thin veins in association with tetrahedrite, galena, sphalerite, and bornite (Eniosova and Mitoyan 2011; Merkel 2016). There were over a dozen other mines documented in the region, and mining in the area was from the 7 to 12th c. CE, although there was a general decline in the 10th c. CE. Merkel also analyzed lead slag from the city of Tunket, located near Almalyk, Uzbekistan. The city, which was occupied from the 4–12th c. CE has extensive evidence of silver production dating from the 9 to 10th c. CE, including more than 4,000 m^3 of slag recovered, large grinding millstones, and cupellation dishes (Merkel 2016). The main group of lead glazes had a strong similarity to the isotopic signatures of the Lashkerek and Tunket slags and ores (Fig. 17).

Throughout the 9th c. CE, there were conflicts between the Samanids in Transoxiana and the Karakhanids in Semirechye (Davidovich 1998). The Samanids in 840 CE started advancing in the Karakhanid region, taking the city of Sayram (Isfijab), and by 893 CE advancing all to Taraz. At the end of the 10th c. CE, the situation shifted with the Karakhanids retaking Sayram in 990, the Ferghana valley in 991–992, and Ilaq, Samarkand, and Bukhara in 992 (Davidovich 1998). The Samanid mines in Transoxiana and Ferghana, including the Lashkerek mine, would have thus come under the control of the Karakhanids at the end of the 10th c. CE and could have been a source of the lead used in the ceramic glazes dated to the 11–12th c. CE.

Samples also had similar isotopic signatures to a known mine in the Semirechye region, Aktyuz, although there are far fewer ore samples from this deposit (Chiaradia et al. 2006). Aktyuz was mined beginning in the 10th c. CE (Merkel 2016)[3] and lies just across the modern Kazakhstan/Kyrgyzstan border from one of the sites in this study, Kastek (Fig. 16). Kastek is located on the northern slope of the Ile Alatau on the left side of the Kystak River in the heartland of the Karakhanid Khaganate. One of the samples with a strong association to the Aktyuz deposit is K200, which was excavated from the ceramic production area at Aktobe, suggesting that potters in the city, which has been identified as the Karakhanid capital of Balasagun, could have obtained some of their lead from local sources. The other two sherds from the Aktobe ceramic production area, K198 and K199, are isotopically distinct from any known silver mine in the region and the only known similar source is the Caixiashan deposit in Xinjiang. This suggests that they were also obtaining lead ore from much further away and that they are not strictly obtaining lead ores from local sources.

The upper courses of the Talas River valley also have evidence of Medieval silver mining, documented by Bubnova (1963). These mines, which would have been the closest sources geographically to the sites in this study, saw an increase of mining occurring in the late 10–11th c. CE under the Karakhanids (Merkel 2016). This increase in mining occurred concurrently with an increase in the presence of glazed ceramics in the region. The mines in this region are described as being decentralized small-scale workings. Pavlova and Borisenko (2009) describe a portion of the Talas ore district including three ore clusters, Babakhan, Kumyshtag, and Kurgan, which lie just north of the Talas-Fergana fault in the Northern Tianshan

[3] http://www.stansenergy.com/K_History.htm

district. However, no isotopic characterizations of lead ores from these mines by LIA is known to date, and this region presents a strong potential for future research.

Other samples

The cluster of eight samples (K050, K066, K068, K088, K183, K195, K198, K199) has a very discrete isotopic signature that matches that of the Caixiashan deposit in the Middle Tianshan district of the Central Asian Orogenic Belt (CAOB) (Fig. 16). Caixiashan is a sediment-hosted Pb–Zn deposit, where the ore is mainly hosted by siliceous clastic rocks and carbonates that generally show no direct genetic association with intrusions (Wang et al. 2020). While the Caixiashan deposit is a strong match to this group of samples, there are still many ore deposits in the region that have not been characterized by LIA.

The two samples that have unique isotopic signatures, K010 and K149, do not have similar isotopic signatures to any distinct ore deposits from the comparative database. However, they both fall within the isotopic fields of districts within the CAOB and the surrounding regions, which allow for some indication of potential sources. K149 (Fig. 3) has a very high-quality lead glaze in the calligraphy style. This style was first produced by the "Samarkand school" and is one of the highest quality Early Islamic ceramics, known for their pure white slip used as the ground, precise painting of the calligraphy, and the brilliance of the transparent lead glaze (Watson 2004, p. 48). The "Samarkand school" ceramics are found throughout Transoxiana and Greater Khorasan and is thought to have been produced in Samarkand and Nishapur (Henshaw 2010). While there was no specific source identified in the database from the known deposits in the Tianshan Belt or any deposits from the geographical region encompassed in the cultural region (Xinjiang, former Soviet republics, and Iran) that was isotopically similar to K149, it falls on the edge of the larger isotopic field of the Balkhash Metallogenic Belt. K010 is more difficult to identify. It falls on the edge of the Southern Tianshan isotopic field and the Beishan isotopic field in the southern CAOB. When comparing to ore deposits from a geographically larger area (see Supplementary Information) K010 (Fig. 3) also has a similar isotopic signature with ore samples from the Deh Hosein deposit in the Sanandaj-Sirjan zone in Iran. Deh Hosein was an ancient Sn-Cu mine; however, there is no evidence for mining in the Medieval Period (Nezafati 2006). All of these regions are potential sources for lead, and further characterization of ore sources in Central Asia is required to confidently identify the source for this sample.

Connections with metallurgy?

Lead sources

It has been hypothesized in the past that litharge from silver cupellation was recycled and used as the raw material for lead glass and glazes (Walton 2009). Litharge contains significant quantities of metals also present in the original ores, including Zn, As, Sn, Bi, Ag, Sb, and Cu (Craddock 1995; Pernicka et al. 1998; L'Heritier et al. 2015). Walton (2004) analyzed the trace elements in a group of Roman lead glazes by electron microprobe to determine if they were rich in the elements believed to favorably partition into litharge during cupellation (Zn, Sb, As, Sn, Ag, and S). The results from this initial study were ambiguous, and no clear evidence was found to identify litharge recycling in lead glazes. While all the samples contained Zn, it was not clear how the Zn related to the PbO raw materials. Sn, Ag, and S were only observed in a few samples, and the pattern appeared incidental. While As and Sb were elevated in some samples and were potentially significant, not enough samples were analyzed to draw conclusions (Walton 2004). In a later study of the lead isotopes in Roman lead-glazed ceramics by Laser ablation TOF-ICP-MS, Walton (2009) identified Spanish ore sources as the potential source for the lead ore in Roman glazed sherds. Given the extensive silver mining activities in the region during the 1st c. CE, Walton suggests that the recycled litharge would have been a logical source for the lead used in the production of lead glaze (Walton 2009). In a recent study of glass production in the 9th c. Iberia, Schibille et al. (2020) identified the use of lead byproducts from silver production for both high-lead glass and soda-ash lead glass. For the high-lead glass, the presence of high levels of Ba and low levels of Ag point to the use of lead slag. For the soda-ash lead glass, much lower levels of Al, Fe, and Ba were observed, but high levels of Cl, Ag, Sn, and Bi suggest the use of litharge from silver cupellation in this glass (Schibille et al. 2020).

The most distinguishing element for the high-lead glaze compositions in this study was bismuth (Fig. 5). High concentrations of bismuth is a distinctive feature in silver from Transoxiana (Merkel 2016). Bismuth was found in all of the galena associations of the Lashkerek mine, and its quantity increased considerably with the depth of the mine (Merkel 2016). The elevated concentrations of Bi in the glazes whose isotopic signature is similar to the deposits in known silver mines further support the hypothesis that the potters where either sourcing the lead rich minerals, such as galena, from these deposits or litharge itself for the production of the lead glaze. The use of the litharge from the silver cupellation for the glaze production would account for the elevated concentrations of Bi in the glazes, as Bi fractionates favorably into the litharge compared to the silver fraction

during cupellation (L'Heritier et al. 2015). While the use of litharge in glaze and glass production warrants further investigation, the results of this initial characterization suggest a link between silver metallurgy and ceramic production in the Early Islamic Period.

Opacifying agents

Connections to metallurgy were drawn in the analysis of the opacifying agents in the glazed ceramics. Antimony and tin, as discussed above, are common elements associated with lead and silver ores. These opacifying agents, especially antimony, have also been hypothesized to be sourced as a byproduct of metallurgical activities. Mass et al. (1998) proposed the source of antimony in opaque Roman glass as litharge from cupellation of antimonial silver ores. Antimony-rich ores were exploited by the Romans for silver production, both in the form of argentiferous lead ores and dry silver ores, which had insufficient lead and required the addition of lead during their processing (Mass et al. 1998). In their analysis of white, turquoise, yellow, and green opaque Roman glasses, they identified the use of both roasted stibnite as an antimony source in the white and turquoise glasses, and the use of litharge contaminated with high levels of antimony, a byproduct of silver production, as the opacifier and colorant in yellow and green glasses (Mass et al. 1998).

Research by Pernicka et al. (1998) and L'Heritier et al. (2015) have shown that antimony and tin oxidize at the beginning of silver cupellation and would be present in the first portion of the litharge. Pernicka et al. (1998) found lead antimonates in archaeological litharges from the first stages of cupellation, with up to 5 wt% Sb_2O_3 measured in the surface of the litharge cakes. L'Heritier et al. (2015) observed SnO_2 and Sb_2O_3 in experimental samples of litharge forming rings of SnO_2-Sb_2O_3, lead antimonate, and lead tin oxide on the outer rim of cupels. The oxidized compounds separate as dross on the surface of the metallic bath and a portion of each element which will stay in solution in the first fraction of the litharge. The dross, which would naturally form when processing Sb-rich lead ores, could be traded as a valuable byproduct of the cupellation. An increase in the investigation of the use and trade of the antimony dross has been suggested in regions with antimony-rich lead ore deposits given the value of the product (L'Heritier et al. 2015, p. 64).

As mentioned above, the main silver ore sources in Central Asia all contain the unusual Ag-Sb mineralization type (Pavlova and Borisenko 2009). These include the Pamir Bazardara ore cluster, and the Kurgan ore cluster in the Talas district, which have Ag-bearing tetrahedrite and stannite minerals associated with them in addition to galena, stibnite, and native silver and antimony (Pavlova and Borisenko 2009). These regions, which were exploited as silver mines in the Medieval Period, would have produced SnO_2-Sb_2O_3, lead antimonate, and lead tin oxide, as dross during silver cupellation.

Metal byproducts, including dross, have been described as components in the production of glass and glazes by Islamic scholars in the 8–14th c. CE. In the treatise *Kitab al-durra al-Maknuna* (8th c.), Jabir ibn-e Hayyan describes the production of colored glass and luster-painted glass. Within the 51 recipes included for glasses in this treatise, he describes coloring agents that are the byproducts of metallurgy including *barani* (dross of brass), *iqlimiya*, which has been identified as gold or dross of silver or gold, as well as copper, tin, and iron filings (Al-Hassan 2009). Another 12th c. CE text, *Jawahir-Nameh-yi Nizami* by Jowhari Nishaburi, dated to 1196 CE, describes the production of luster decoration on ceramics and glass. Translated by Matin (2020), it details twenty-six recipes for luster decoration on ceramics and glass, which detail the materials needed to produce deep red, red, gold, black, silver, yellow, green, and blue decorations. Silver containing compounds are frequently referred to in the treatise, and the recipes mention *ghilimiya-yi fideh* and *ghilimiya-yi zahbi*, which has been identified as slags and waste materials from silver and gold smelting, respectively (Matin 2020, p. 486). Abu'l-Qasim Kashani (1301) also describes colorants for glazes that were described as metalworking byproducts, including copper hammerscale and the scales of burnt iron (Watson 2004). These scholars, who were writing during the Medieval Period in Central and Southwest Asia, provide valuable insights into the craft production of the period and documented the link between metallurgy and ceramic and glass production.

Elevated concentrations of antimony (~0.3 wt% Sb_2O_5) in some transparent lead glazes (K047, K050, and K067) and the use of antimony based opacifiers in the opaque glazes (K010, K106, K178, K185, K196, K205, K212, and K213) suggest the use of antimony-rich lead ores and metallurgical byproducts by potters in the region. The use of antimony-rich lead ores would result in elevated concentrations of antimony in the lead glazes. The use of antimony-based opacifiers, which has previously not been noted in lead glazes the eastern Islamic world in this period, is most likely explained by the use of the antimony-rich dross from silver cupellation. This would be both a more convenient and economical opacifier than tin, which according to the Abu'l-Qasim Kashani in 1301 CE was imported to Northern Iran either from Farangistan (understood to be Europe), China, or Bulghars (land north of the Caucasus region) (Allan 1973; Matin 2020). The presence of both SnO_2 and Sb_2O_5 in opaque glazes (K010, K185, K205, and K212) also supports this hypothesis, as

ores rich in tin and antimony would result in the formation of SnO_2-Sb_2O_3, lead antimonate, and lead tin oxide in the dross (L'Héritier et al. 2015).

Conclusions

Chemical compositional analysis of ninety-five glazed ceramics from the 9–15th c. CE in southern Kazakhstan identified several distinct glaze types including transparent high-lead glaze, opaque high-lead glaze, low-lead glaze, and alkali-fluxed glaze. The majority of the glazed ceramics from southern Kazakhstan have a transparent high-lead glaze, which have a very uniform composition and are similar to other Central Asia sites in the Early Islamic Period. No chemical differentiation was observed between glazes of different periods of production, provenance, or ware when colorants are removed. For the locally produced ceramics in southern Kazakhstan, only copper, iron, and manganese were observed as colorants, which were commonly used on Early Islamic lead-glazed ceramics from across the Islamic world. Two colorants, cobalt and chromium, were only observed on non-local ceramics.

Three different opaque glazes were identified: tin-opacified glazes, tin- and antimony-opacified glazes, and antimony-opacified glazes. The occurrence of antimony-opacified glazes, and tin- and antimony-opacified glazes is unattested in this region in the Early Islamic Period and indicates that the local craftsmen in southern Kazakhstan are innovating in their production of opaque-glazed ceramics. Antimony, both raw antimony and stibnite, is available in northern Central Asia in silver-antimony deposits in the Tianshan and Pamir silver ore districts. We do not think this is linked to the reintroduction of antimony in Egypt in the 9th c. CE but as a parallel case of craftsmen experimenting with local raw materials to create opaque glazed ceramics. While more research needs to be done, the presence of tin- and antimony-opacified glazes could be the result of using antimony- and antimony-tin-rich dross from silver cupellation.

This is the first application of lead isotope analysis to glazed ceramics from northern Central Asia. The distribution of the isotopic signatures suggests that the craftspeople were obtaining lead from at least two different sources for their glazed production. Using a comparative database, we were able to identify compatible ore sources for the majority of our samples from within the southern CAOB. The main group of samples had an isotopic signature that fell within the isotopic fields of the Tianshan districts. Through the application of the Euclidean distance, we were able to identify potential ore deposits, including deposits that were known silver mines during the Medieval Period. These ore sources were local and suggest that the potters were obtaining the lead for glaze production from within larger acquisition networks. The high levels of bismuth identified in the glazes also reinforce this conclusion, as the silver from the Tianshan mountains in the Transoxiana region is known for uniquely high levels of bismuth. The high levels of bismuth also could suggest the use of litharge from silver cupellation as the raw material for the lead glazes, and although this warrants further investigation, the results of this initial characterization suggest a link between silver metallurgy and ceramic production in the Early Islamic Period. One cluster of eight samples had a distinct isotopic signature that matched a unique deposit in Xinjiang, China. While this does not unequivocally prove that potters were sourcing lead from this deposit given the large number of uncharacterized lead deposits in the region, it does strongly suggest craftsmen were also sourcing lead ore from much further away and that they are not strictly obtaining lead ores from local sources.

Supplementary Information The online version contains supplementary material available at https://doi.org/10.1007/s12520-021-01444-8.

Acknowledgements The Institute of Archaeology of Kazakhstan provided the ceramics for analysis, and we thank them for their ongoing support and collaboration. We would like to extend our thanks to the two anonymous referees for their valuable comments on this article. The authors would like to thank Brandi MacDonald for her thoughtful feedback and Laure Dussubieux for her assistance with the LA-ICP-MS and her feedback on the article. We are grateful to Jay Stephens and Mark Baker (University of Arizona) for their assistance with the lead isotope sampling. We are also grateful to Dr. Kenneth Domanik (Electron Microprobe Lab, Lunar and Planetary Science Department, University of Arizona) for assistance with the electron microprobe analysis.

Author contribution C. Klesner designed the project with input from D. Killick and V. Renson. Y. Akymbek provided the samples and contributed information on the archaeological context. Sample preparation and microprobe analyses were conducted by C. Klesner. V. Renson carried out the MC-ICP-MS analyses. The manuscript was written by C. Klesner, and all authors contributed to sections of the manuscript. All authors reviewed and approved the manuscript before submission.

Funding This research was funded through the National Science Foundation (grant #BCS-1916298). The Archaeometry Laboratory at MURR is supported by the National Science Foundation (grant #BCS-1912776), and the acquisition of the Nu Plasma II MC-ICP-MS at MURR was funded by the National Science Foundation (grant #BCS-0922374). The acquisition of the Thermo ICAP Q ICP-MS at the Field Museum was funded by the NSF (grant #BCS-1531394).

Availability of data and material The data used for this work is included in the Supplementary Material.

Code availability Not applicable.

Declarations

Conflict of interest The authors declare no competing interests.

References

Akylbek SS, Smagulov EA, Yatsenko SA (2017) Decor of the Eigth-Century Turkic Rulers' Residence in the Citadel of Kulan Town. Silk Road 15:65–82

Akymbek Y, Baibugunov B (2014) Inscriptions on ceramics of Medieval City Aktobe. Procedia - Soc Behav Sci 122:77–81. https://doi.org/10.1016/j.sbspro.2014.01.1306

Alexeiev DV, Kroner A, Hegner E et al (2016) Middle to Late Ordovician arc system in the Kyrgyz Middle Tianshan: from arc-continent collision to subsequent evolution of a Palaeozoic continental margin. Gondwana Res 39:261–291. https://doi.org/10.1016/j.gr.2016.02.003

Al-Hassan A (2009) An Eighth Century Arabic Treatise on the Colouring of Glass: Kitab al-Durra al-Maknuna (The Book of the Hidden Pearl) of Jabir Ibn Hayyah (c. 721-c. 815). Arab Sci Philos 19:121–156. https://doi.org/10.1017/S0957423909000605

Allan JW (1973) Abū'l-Qāsim's Treatise on Ceramics. Iran 11:111–120

Allan JW (1991) Islamic ceramics. Oxford

Allan JW, Llewellyn LR, Schweizer F (1973) The history of so-called Egyptian Faience in Islamic Persia: investigations into Abū'l-Qāsim's Treatise. Archaeometry 2:165–173

Barisitz S (2017) Central Asia and the Silk Road economic rose and decline over several millennia. Springer, Cham, Switzerland

Baxter MJ, Buck CE (2000) Data handling and statistical analysis. In: Ciliberto E, Spoto G (eds) Modern Analytical Methods in Art and Archaeology. pp 681–746

Baxter MJ (1992) Archaeological uses of the biplot—a neglected technique? In: Lock G, Moffett J (eds) Computer Applications and Quantitative Methods in Archaeology, 1991. pp 141–143

Bouquillon A, Coquinot Y, Doublet C (2012) Chapter III Pottery study and analyses. In: Rante R, Collinet A (eds) Nishapur Revisited: Stratigraphy and Ceramics of the Qohandez. Oxbow Books, Oxford, pp 56–135

Brill RH, Felker-Dennis C, Shirahata H, Joel EC (1997) Lead isotope analyses. In: Conservation of Ancient Sites on the Silk Road. The Getty Conservation Institute, Los Angeles, pp 369–378

Brunet M-F, Sobel E, McCann T (2017) Geological evolution of Central Asian Basins and the Western Tien Shan Range. Geol Soc London 427:1–17. https://doi.org/10.1144/SP427.17

Cao C, Shen P, Pan H et al (2018) Fluid evolution and mineralization mechanism of the East Kounrad porphyry Mo-W deposit in the Balkhash metallogenic belt, Central Kazakhstan. J Asian Earth Sci 165:175–191. https://doi.org/10.1016/j.jseaes.2018.07.013

Chegini NN, Momenzadeh M, Parzinger H et al (2000) Preliminary report on archaeometallurgical investigations around the prehistoric site of Arisman near Kashan, western Central Iran. Archaeol Mitteilungen Aus Iran Und Turan 32:281–318

Chen HY, Chen YJ, Baker M (2012) Isotopic geochemistry of the Sawayaerdun orogenic-type gold deposit, Tianshan, northwest China: implications for ore genesis and mineral exploration. Chem Geol 310–311:1–11. https://doi.org/10.1016/j.chemgeo.2012.03.026

Chernyshev IV, Golubev VN, Chugaev AV (2017) Anomalous lead isotopic composition of Galena and age of altered uranium minerals: a case study of Chauli Deposits, Chatkal-Qurama District, Uzbekistan. Geol Ore Depos 59:551–560. https://doi.org/10.1134/S107570151706006X

Chiaradia M, Konopelko D, Seltmann R, Cliff RA (2006) Lead isotope variations across terrane boundaries of the Tien Shan and Chinese Altay. Miner Depos 41:411–428. https://doi.org/10.1007/s00126-006-0070-x

Craddock PT (1995) Lead and silver. Early Metal Mining and Production. Edinburgh University Press, Edinburgh, pp 205–233

Cui JF, Lei Y, Jin ZB et al (2010) Lead isotope analysis of tang sancai pottery glazes from Gongyi Kiln, Henan Province and Huangbao Kiln, Shaanxi Province. Archaeometry 52:597–604. https://doi.org/10.1111/j.1475-4754.2009.00495.x

Davidovich EA (1998) The Karakhanids. In: Asimov MS, Bosworth CE (eds) The history of civilizations of Central Asia, vol IV. UNESCO Publishing, Paris, pp 125–149

Ding Q-F, Wu C-Z, Santosh M et al (2014) H-O, S and Pb isotope geochemistry of the Awanda gold deposit in southern Tianshan, Central Asian orogenic belt: implications for fluid regime and metallogeny. Ore Geol Rev 62:40–53. https://doi.org/10.1016/j.oregeorev.2014.02.017

Dolgopolova A, Seltmann R, Konopelko D, et al (2017) Geodynamic evolution of the western Tian Shan, Uzbekistan: insights from U-Pb SHRIMP geochronology and Sr-Nd-Pb-Hf isotope mapping of granitoids. Gondwana Res 47:76–109. dx.doi.org/https://doi.org/10.1016/j.gr.2016.10.022

Ehya F (2014) The Paleozoic Ozbak-Kuh carbonate-hosted Pb-Zn deposit of East Central Iran: isotope (C, O, S, Pb) geochemistry and ore genesis. Mineral Petrol 108:123–136. https://doi.org/10.1007/s00710-013-0279-1

Eniosova N, Mitoyan R (2011) Arabic coins as a silver source for Slavonic and Scandinavian Jewellers in the Tenth Century AD. In: Turbanti-Memmi I (ed) Proceedings of the 37th International Symposium on Archaeometry. Springer, pp 579–584

Galer SJG, Abouchami W (1998) Practical application of lead triple spiking for correction of instrumental mass discrimination. Mineral Mag 62A:491–492

Gradmann R, Berthold C, Schüssler U (2015) Composition and colouring agents of historical Islamic glazes measured with EPMA and μ-XRD2. Eur J Mineral 27:325–335. https://doi.org/10.1127/ejm/2015/0027-2456

Hallett JR, Thompson M, Keall EJ, Mason RB (1988) Archaeometry of medieval Islamic glazed ceramics from North Yemen. Can J Chem 66:266–272. https://doi.org/10.1139/v88-045

Heinsch M, Vandiver PB, Lyublyanovics K, et al (2018) Ceramics at the emergence of the Silk Road: a case from southeastern Kazakhstan. Mater Issues Art Archaeol X MRS Sympos:251–282

Henshaw CM (2010) Early Islamic ceramics and glazes of Akhsiket. University College London, Uzbekistan

Henshaw CM, Rehren T, Anarbaev A (2006) The early Islamic glazed ceramics of Akhsiket, Uzbekistan. 34th Int Symp Archaeom 3–7 May 2004, Zaragoza, Spain 489–493

Holakooei P, de Lapérouse JF, Carò F et al (2019) Non-invasive scientific studies on the provenance and technology of early Islamic ceramics from Afrasiyab and Nishapur. J Archaeol Sci Reports 24:759–772. https://doi.org/10.1016/j.jasrep.2019.02.029

Hong D, Wang S, Xie X et al (2003) Metallogenic province derived from mantle sources: Nd, Sr, S and Pb isotope evidence from the Central Asian Orogenic belt. Gondwana Res 6:711–728. https://doi.org/10.1016/s1342-937x(05)71019-4

Hsu YK, Sabatini B (2019) A geochemical characterization of lead ores in China: an isotope database for provenancing archaeological materials. PLoS ONE 14:e0215973. https://doi.org/10.1371/journal.pone.0215973

Huntley DL, Fenn TR, Habicht-Mauche JA, Mills BJ (2012) Embedded networks? Pigments and long-distance procurement strategies in the Late Prehistoric Southwest. In: Cordell LS, Habicht-Mauche JA (eds) Potters and Communities of Practice: Glaze Paint and Polychrome Pottery in the American Southwest, A.D. 1250 to 1700, Number 75. Anthropological Papers of The University of Arizona, Tucson, AZ, pp 8–18

Jenchuraeva RJ (1997) Tectonic settings of porphyry-type mineralization and hydrothermal alteration in Paleozoic island arcs and active continental margins, Kyrghyz Range, (Tien Shan)

Kyrghyzstan. Miner Depos 32:434–440. https://doi.org/10.1007/s001260050111
Jepson G, Glorie S, Konopelko D et al (2018) Low-temperature thermochronology of the Chatkal-Kurama Terrane (Uzbekistan-Tajikistan): insights into the Meso-Cenozoic thermal history of the Western Tian Shan. Tectonics 37:1–17. https://doi.org/10.1029/2017TC004878
Killick D, Stephens JA, Fenn TR (2020) Geological constraints on the use of lead isotopes for provenance in archaeometallurgy. Archaeometry 62:86–105. https://doi.org/10.1111/arcm.12573
Klesner CE, MacDonald BL, Dussubieux L et al (2019) Local production and long-distance trade of Islamic glazed ceramics in Central Asia: a compositional analyses of ceramics from Southern Kazakhstan by NAA and LA-ICP-MS. J Archaeol Sci Reports 26:101905. https://doi.org/10.1016/j.jasrep.2019.101905
Klesner CE, Akymbek Y, Vandiver PB (2021) Lead-glazing technology from Medieval Central Asia: a case study from Aktobe. Kazakhstan J Archaeol Sci 36:102825. https://doi.org/10.1016/j.jasrep.2021.102825
Klesner CE (2021) The regional production, consumption, and trade of glazed ceramics in Medieval Central Asia. The University of Arizona
Kroner A (2015) The Central Asian Orogenic Belt - present knowledge and comparison with the SW Pacific. In: Kroner A (ed) The Central Asian Orogenic Belt: Geology, Evolution, Tectonics and Models. Borntraeger Science Publishers, Stuttgart, pp 1–5
L'Heritier M, Baron S, Cassayre L, Tereygeol F (2015) Bismuth behaviour during ancient processes of silver-lead production. J Archaeol Sci 57:56–68. https://doi.org/10.1016/j.jas.2015.02.002
Li D, Chen H, Hollings P et al (2018) Isotopic footprints of the giant Precambrian Caixiashan Zn-Pb mineralization system. Precambrian Res 305:79–90. https://doi.org/10.1016/j.precamres.2017.11.014
Lu WJ, Zhang L, Chen HY et al (2018) Geology, fluid inclusion and isotope geochemistry of the Hongyuan reworked sediment-hosted Zn–Pb deposit: metallogenic implications for Zn–Pb deposits in the Eastern Tianshan, NW China. Ore Geol Rev 100:504–533. https://doi.org/10.1016/j.oregeorev.2017.01.004
Martínez Ferreras V, Fusaro A, Gurt Esparraguera JM et al (2019) The Islamic Ancient Termez through the lens of ceramics: a new archaeological and archaeometric study. Iran 0:1–29. https://doi.org/10.1080/05786967.2019.1572430
Marzo P, Laborda F, Perez-Arantegui J (2009) Medieval and postmedieval Hispano-Moresque glazed ceramics: new possibilities of characterization by means of lead isotope ratio determination by Quadrupole ICP-MS. In: Degryse P, Henderson J, hod (eds) Isotopes in Vitreous Materials. Leuven University Press, Leuven, Belgium, pp 131–144
Mason RB (1995) New looks at old pots. Muqarnas 12:1–10
Mason RB, Farquhar RM, Smith PE (1992) Lead-isotope analysis of Islamic glazes: an exploratory study. Muqarnes 9:67–71
Mass JL, Stone RE, Wypyski MT (1998) The mineralogical and metallurgical origins of Roman opaque colored glasses. In: McCray P, Kingery WD (eds) The Prehistory & History of Glassmaking Technology. The American Ceramic Society Inc, Westerville, OH, pp 121–144
Matin M (2019) Tin-based opacifiers in archaeological glass and ceramics glazes: a review and new perspectives. Archaeol Anthropol Sci 11:1155–1167. https://doi.org/10.1007/s12520-018-0735-2
Matin M (2020) Appendix: The technology of Medieval Islamic ceramics: a study of two Persian manuscripts. Ceramics From Iran. Yale University Press, New Haven, CT, pp 459–487
Matin M, Tite M, Watson O (2018) On the origins of tin-opacified ceramic glazes: new evidence from early Islamic Egypt, the Levant, Mesopotamia, Iran, and Central Asia. J Archaeol Sci 97:42–66. https://doi.org/10.1016/j.jas.2018.06.011
Medeghini L, Fayek M, Mignardi S et al (2020) A provenance study of Roman lead-glazed ceramics using lead isotopes and secondary ion mass spectrometry (SIMS). Microchem J 154:104519. https://doi.org/10.1016/j.microc.2019.104519
Merkel SW (2016) Silver and the silver economy at Hedeby. VML Verlag Marie Leidorf, Bochum, Germany
Molera J, Coll J, Labrador A, Pradell T (2013) Manganese brown decoration in 10th to 18th century Spanish tin glazed ceramics. Appl Clay Sci 82:86–90
Molera J, Martínez Ferreras V, Fusaro A, et al (2020) Islamic glazed wares from ancient Termez (southern Uzbekistan). Raw materials and techniques. J Archaeol Sci Reports 29:102169. https://doi.org/10.1016/j.jasrep.2019.102169
Neff H (1994) RQ-Mode principal components analysis of ceramics compositional data. Archaeometry 1:115–130
Neff H (2002) Quantitative techniques for analyzing ceramic compositional data. In: Glowacki DM, Neff H (eds) Ceramic Source Determination in the Greater Southwest: Source Determination by INAA and complementary mineralogical investigations, Monograph. Costen Institute of Archaeology, UCLA, pp 15–36
Nezafati N (2006) Au-Sn-W-Cu-mineralization in the Astaneh-Sarband Area. University of Tübingen, West Central Iran including
Oka R, Dussubieux L, Kusimba C, Gogte VD (2009) The impact of "Imitation" Celadon and Blue-and-White Industries on Chinese ceramic exports in the Indian Ocean Maritime Exchange, ca. 1200–1700 C.E. In: McCarthy BE, Chase E, Cort L, et al. (eds) Scientific Research on Historic Asian Ceramics: Proceedings of the Fourth Forbes Symposium at the Freer Gallery of Art. Freer Gallery of Art, Smithsonian Institution, Washington D.C., pp 175–185
Pavlova GG, Borisenko AS (2009) The age of Ag-Sb deposits of Central Asia and their correlation with other types of ore systems and magmatism. Ore Geol Rev 35:164–185. https://doi.org/10.1016/j.oregeorev.2008.11.006
Pernicka E, Rehren T, Schmitt-Strecker S (1998) Late Uruk silver production cupellation Habuba Kabira, Syria. Metall Antiq 8:123–134
Pernicka E, Malissa H (1980) Examination of Islamic glazes with the electron microprobe. In: Slater EA, Tate JO (eds) Proceedings of the sixteenth international symposium of archaeometry and archaeological prospection. National Museum of Antiquities of Scotland, Edinburgh, pp 96–112
Pernicka E, Adam K, Bohme M, et al (2011) Archaeometallurgical research on the western Central Iranian Plateau. In: Vatandoust A, Parzinger H, Helwing B (eds) Early mining and metallurgy on the Western Central Iranian Plateau: the first five years of work. Archäologie in Iran und Turan, pp 633–705
Pollard AM, Batt CM, Stern B, Young SMM (2007) Analytical chemistry in archaeology. Cambridge University Press, Cambridge, UK
Puschnigg G, Houal J-B (2019) Regions and regional variations in Hellenistic Central Asia: what pottery assemblages can tell us. Afghanistan 2:115–140. https://doi.org/10.3366/afg.2019.0028
Salinas E, Pradell T, Matin M, Tite M (2019) From tin- to antimony-based yellow opacifiers in the early Islamic Egyptian glazes: regional influences and ruling dynasties. J Archaeol Sci Reports 26:101923. https://doi.org/10.1016/j.jasrep.2019.101923
Santarelli B (2015) Technological analysis of Pueblo I lead glazed ceramics from the Upper San Juan Basin , Colorado (ca . 700–850 CE). The University of Arizona
Schibille N, Ares JDJ, Casal Garcia MT, Guerrot C (2020) Ex novo development of lead glassmaking in early Umayyad Spain. PNAS 117:16243–16249. https://doi.org/10.1073/pnas.2003440117
Shalekenov UK (2009) Balasagun city in the 5–13 centuries. Almaty, Kazakhstan
Shen JY, Henderson J, Evans J et al (2019) A study of the glazing techniques and provenances of Tang sancai glazes using elemental

and lead isotope analyses. Archaeometry 61:358–373. https://doi.org/10.1111/arcm.12436
Shen P, Pan H, Li Z et al (2020) A Manto-type Cu deposit in the Central Asian Orogenic Belt: the Hongguleleng example (Xinjiang, China). Ore Geol Rev 124:103656. https://doi.org/10.1016/j.oregeorev.2020.103656
Shen J (2017) Chemical and isotopic analysis in the investigation of glazes from Northern China and the chemical and isotopic analysis in the investigation of glazes from Northern China and the Middle East , 7th-14th centuries AD. The University of Nottingham
Shortland A (2002) The use and origin of Antimonate colorants in Early Egyptian glass. Archaeometry 44:517–530
Stos-Gale S (2004) Lead-isotope analyses of glass, glazes, and some metal artifacts. Serçe Limani: An Eleventh-Century Shipwreck. Texas A&M University Press, College Station, TX, pp 453–467
Syromyatnikov NG, Kolesnikov VV et al (1988) Time of formation of porphyry copper deposits in Kazakhstan by isotopic composition of lead ore. Geokhimiya 1:3–14 (**in Russian**)
Thibodeau AM, Chesley JT, Ruiz J (2012) Lead isotope analysis as a new method for identifying material culture belonging to the Vázquez de Coronado expedition. J Archaeol Sci 39:58–66. https://doi.org/10.1016/j.jas.2011.07.025
Thibodeau AM, Habicht-Mauche JA, Huntley DL et al (2013) High precision isotopic analyses of lead ores from New Mexico by MC-ICP-MS: Implications for tracing the production and exchange of Pueblo IV glaze-decorated pottery. J Archaeol Sci 40:3067–3075. https://doi.org/10.1016/j.jas.2013.02.034
Ting C, Taxel I (2020) Indigeneity and innovation of early Islamic glaze technology: the case of the Coptic Glazed Ware. Archaeol Anthropol Sci 12. https://doi.org/10.1007/s12520-019-01007-y
Tite M (1989) Iznik pottery: an investigation of the methods of production. Archaeometry 31:115–132
Tite MS (2011) The technology of glazed islamic ceramics using data collected by the late Alexander Kaczmarczyk. Archaeometry 53:329–339. https://doi.org/10.1111/j.1475-4754.2010.00546.x
Tite MS, Freestone I, Mason R et al (1998) Lead glazes in antiquity - methods of production and reasons for use. Archaeometry 40:241–260. https://doi.org/10.1111/j.1475-4754.1998.tb00836.x
Tite M, Watson O, Pradell T et al (2015) Revisiting the beginnings of tin-opacified Islamic glazes. J Archaeol Sci 57:80–91. https://doi.org/10.1016/j.jas.2015.02.005
Walton MS (2009) PLS regression to determine lead isotope ratios of Roman lead glazed ceramics by laser ablation TOF-ICP-MS. In: Degryse P, Henderson J, Hodgins G (eds) Isotopes in Vitreous Materials. Leuven University Press, Leuven, Belgium, pp 145–161
Walton MS, Tite MS (2010) Production technology of roman lead-glazed pottery and its continuance into late antiquity. Archaeometry 52:733–759. https://doi.org/10.1111/j.1475-4754.2009.00506.x
Walton MS (2004) A materials chemistry investigation of archaeological lead glazes. University of Oxford
Wang G-N, Gu X-X, Zhang Y-M et al (2018) Ore genesis and hydrothermal evolution of the Kendenggao'er copper-molybdenum deposit, western Tianshan: evidence from isotopes (S, Pb, H, O) and fluif inclusions. Ore Geol Rev 100:294–316. https://doi.org/10.1016/j.oregeorev.2018.01.004
Wang K, Wang Y, Xue C et al (2020) Fluid inclusions and C-H-O-S-Pb isotope systematics of the Caixishan sediment-hosted Zn-Pb deposit, eastern Tianshan, northwest China: implication for ore genesis. Ore Geol Rev 119:103404. https://doi.org/10.1016/j.oregeorev.2020.103404
Watson O (2020) Ceramics of Iran. Yale University Press, New Haven, CT
Watson O (2004) Ceramics from Islamic lands. Thames and Hudson, Ind., New York
Watson O (2014) Revisiting Samarra: the rise of Islamic glazed pottery. In: Gonnella, J., Abdellatif, R., Struth S (ed) Beiträge zur Islamischen Kunst und Archäologie 4. pp 125–144
Weis D, Kieffer B, Maerschalk C et al (2006) High-precision isotopic characterization of USGS reference materials by TIMS and MC-ICP-MS. Geochemistry Geophys Geosystems 7:1–30. https://doi.org/10.1029/2006GC001283
Wilkinson CK (1975) Nishapur: pottery of the Early Islamic Period. The Metropolitan Museum of Art, New York
Wolf S, Stos S, Mason R, Tite MS (2003) Lead isotope analyses of Islamic pottery glazes from Fustat. Egypt Archaeometry 45:405–420. https://doi.org/10.1111/1475-4754.00118
Zhang Z-J, Chen H, Hu M-Y et al (2014) Isotopic geochemistry of the Jinwozi gold deposit in the eastern Tianshan orogen, NW China: implications for the ore genesis. Geol J 49:574–583. https://doi.org/10.1002/gj.2593
Zhang L, Chen H, Liu C, Zheng Y (2018) Ore genesis of the Saridala gold deposit, Western Tianshan, NW China: constraints from fluid inclusion, S-Pb isotopes and 40Ar/39Ar dating. Ore Geol Rev 100:63–76. https://doi.org/10.1016/j.oregeorev.2017.06.011
Zhao X, Xue C, Chi G et al (2018) Diabase-hosted copper mineralization in the Qunjsai deposit, West Tianshan, NW China: Geological, geochemical and geochronolgical characteristics and mineralization mechanism. Ore Geol Rev 92:430–448. https://doi.org/10.1016/j.oregeorev.2017.11.034